University of Alberta

HYDROENTANGLEMENT AND FIBRE ORIENTATION STUDY ON HEMP BAST FIBRE SLURRY

by Sandeep Singh Randhawa 

A thesis submitted to the Faculty of Graduate Studies and Research in partial fulfillment

of the requirements for the degree of Master of Science

in

Chemical Engineering

Department of Chemical and Materials Engineering

Edmonton, Alberta

Spring 2006

Your file Votre référence
ISBN: 0-494-13878-5
Our file Notre référence
ISBN: 0-494-13878-5

Abstract

Decreasing forest area and environmental concerns over common disposal practices used for agriculture fibres are forcing the forest product industry to look into other fibre resources in addition to wood. One of the promising non-wood fibre source available in Canada is Hemp. Long and strong hemp bast fibres have the potential to increase the strength of paper cost effectively. Hemp bast fibres along with their strength and length advantages also bring some process problems. Hemp bast fibres have inherent tendency to get hydroentangled which gives rise to flow properties different from wood fibre suspensions. Hydroentangled fibres are hard to distribute uniformly which cause plugging of headbox and non-uniform paper formation.

The objective of this work is to understand the effects of various process variables on hydroentanglement and orientation of hemp bast fibres. In this study, image analysis techniques are used to examine the dependence of hydroentanglement and fibre orientation on fibre length, consistency and hydrodynamic conditions.

Acknowledgements

I express my gratitude to my supervisor, Dr. Shijie Liu and to my co-supervisor Mr. Wade Chute for their guidance and support. I am in great debt to Dr. K Nandakumar for his help and encouragement.

I thank the personnel from instrumentation and machine shop, especially Mr. Walter Boddez and Mr. Clark Bicknell for their patience and effort that were key to this thesis.

Finally, I would like to thank the Alberta Research Council for their partial financial support.

Table of Contents

Chapter 1. Introduction

1.1. Nonwood Fibre Sources....2

1.1.1 Industrial Hemp (Cannabis sativa)....2

1.1.2 Flax....3

1.2. Nonwood Fibre Characteristics....5

1.3. Objectives of the Thesis Work....7

1.4 Thesis Layout....8

Chapter 2. Literature Review

2.1 Factors Affecting Flow of Fibre Suspension in Pipe....9

2.1.1 Fibre properties....9

2.1.2 Pulp consistency or concentration of fibres....11

2.1.3 Fibre interaction with fines, coagulants, flocculants and air bubbles....12

2.1.4 Fluid properties....12

2.1.5 Pipe surface roughness....12

2.2 Parameters to Characterize Fibre entanglement and Flocculation....13

2.3 Fibre Orientation....14

Chapter 3. Experimental Design

3.1 Experimental Setup....16

3.2 Hemp Fibre Processing....17

3.2.1 Retting Process 17

3.2.2 Raw material preparation 17

3.2.3 Cooking of hemp fibre 18

3.2.4 Fibre suspension preparation 18

3.3 Data Collection 20

3.4 Data Processing 20

3.4.1 Intensity method 21

3.4.2 Fourier transform method 28

Chapter 4. Results and Discussion

4.1 Pressure drop 33

4.2 Intensity method 39

4.3 Fourier transform method 46

Chapter 5. Conclusions 53

Chapter 6. Future Work 54

References 55

Appendix [A] 57

Appendix [B] 60

Appendix [C] 63

List of Tables

Table 1-1. Physical characteristics of common fibres 5

Table 1-2. Chemical characteristics of common fibres 6

List of Figures

Figure 3-1. Schematic of experimental setup 16

Figure 3-2. Difference vs. Image frames plot for 0.01% softwood fibre suspension 22

Figure 3-3. 0.01% softwood fibre suspension at Reynolds number of 5900 22

Figure 3-4. Difference vs. Image frames plot for 0.01% hemp fibre suspension 23

Figure 3-5. Image frame corresponding to point 1 in Figure.3-4 24

Figure 3-6. Image frame corresponding to point 2 in Figure.3-4 24

Figure 3-7. Image frame corresponding to point 3 in Figure.3-4 25

Figure 3-8. Image frame corresponding to point 4 in Figure.3-4 25

Figure 3-9. Image frame corresponding to point 5 in Figure.3-4 26

Figure 3-10. Image frame corresponding to point 6 in Figure.3-4 26

Figure 3-11. Sample image of hemp fibre bundles 31

Figure 3-12. Edge thresholded image of Figure.3-11 31

Figure 3-13. Fibre orientation distribution of sample image 32

Figure 4-1. Effect of fibre length on friction factor for 0.01% fibre suspension 34

Figure 4-2. Effect of fibre length on friction factor for 0.02% fibre suspension 35

Figure 4-3. Variation in friction factor for 0.01% fibre suspension 36

Figure 4-4. Variation in friction factor for 0.02% fibre suspension 36

Figure 4-5. Effect of consistency on variation in friction factor for 10 mm cut hemp fibres....37
Figure 4-6. Effect of consistency on variation in friction factor for uncut hemp fibres....38
Figure 4-7. Hydroentanglement instances per unit mass for 0.01% hemp fibre suspension....39
Figure 4-8. Hydroentanglement instances per unit mass for 0.02% hemp fibre suspension....40
Figure 4-9. Hydroentanglement instances per unit volume for hemp fibre suspension with 10 mm cut fibres....41
Figure 4-10. Hydroentanglement instances per unit volume for hemp fibre suspension with 5 mm cut fibres....42
Figure 4-11. Hydroentanglement instances per unit mass for hemp fibre suspension with 10 mm cut fibres....42
Figure 4-12. Hydroentanglement instances per unit mass for hemp fibre suspension with 5 mm cut fibres....43
Figure 4-13. Size of hydroentangled fibre flocs for different fibre length....44
Figure 4-14. Size of hydroentangled fibre flocs for fibre suspension with 10 mm cut hemp fibres at different consistencies....44
Figure 4-15. Fibre orientation distribution for softwood fibres....46
Figure 4-16. Standard deviation for various points in Figure.4-15....47
Figure 4-17. Fibre orientation distribution for 5 mm cut hemp fibres....47
Figure 4-18. Standard deviation for various points in Figure.4-17....48

Figure 4-19. Fibre suspension containing 5 mm cut hemp fibres at Reynolds number of 4325 49

Figure 4-20. Edge thresholded image of Figure.4.19 49

Figure 4-21. Fibre suspension containing (hydroentangled) 5 mm cut hemp fibres at Reynolds number of 4325 50

Figure 4-22. Edge thresholded image of Figure.4-21 50

Figure 4-23. Fibre orientation distribution of 10 mm cut hemp fibres 51

Figure 4-24. Standard deviation for various points in Figure.4-23 52

Nomenclature

C_o .....critical concentration

d.....diameter of fibre

L .....length of fibre

N .....crowding factor

C_v.....volumetric concentration of fibres

C_m.....mass consistency

ω .....fibre coarseness

n_c .....number of contacts per fibre

W_1.....initial weight of sample

W_2.....dry weight of sample

w.....weight of the moisture –free pad and filter paper

f .....weight of the moisture –free filter paper

g.....net weight of the original sample

Chapter 1. Introduction

Wood fibres have been the dominant source for papermaking in North America. Decreasing forest area around the world and environmental concerns over common disposal practices used for agriculture fibres are forcing forest product industry to look into alternative fibre resources. Availability and annual renewability make non-wood fibres sources like wheat straw, hemp, flax and corn stalk good alternatives to wood. Agriculture fibres or non-wood plant fibres have potential to increase the fibre supply tremendously. This promoted more and more researchers to look for better management and use of non-wood plant fibres in forest products industry.

The major advantages of non-wood plant fibres are

1. Non–wood plant have short growing period, most of them are annual plants.
2. Bast fibre plants have special fibre properties like longer fibre length, greater tensile strength etc.
3. Use of non-wood plant fibres is economically beneficial for farmers. As this will give them an additional source of income through selling of residual straw.
4. Most of agricultural residues like wheat straw, flax straw, corn stalks are burned for disposal. This is wastage of the resources. In some areas of southern Saskatchewan and Manitoba, burning of flax straw creates hazardous conditions for highway drivers. The use of this material in forest product industry will be environmentally beneficial.

1.1. Non –wood fibre sources

The main non-wood fibre sources in Canada are

1. Common non-woods or hardwood substitutes: - Cereal straw, Grasses etc.
2. Specialty non-woods or softwood substitutes: - Flax, Hemp bast fibres etc.

Paper has been made from non-wood fibres since ancient times. But today, wood fibres have become the major source of papermaking raw material. The use of non-wood plants in papermaking is dependent on availability of wood in most of the countries. The countries in which non-wood fibers are widely used are characterized by wood scarcity. China, India and Pakistan are the three top countries in production of non-wood pulp. Commonly used non-wood fibre sources in these countries are wheat and rice straw, bagasse and bamboo. Paper mills in these countries still need to purchase wood pulp to strengthen paper.

In Canada, wood is the major source of papermaking raw material. Most of research in Canada in non-wood fibre area is focused on specialty non–woods. Specialty non-woods with their peculiar properties have potential to impart unique strength and texture to paper. The common specialty non –wood plants in Canada are Hemp and Flax.

1.1.1. Industrial Hemp (Cannabis sativa)

The hemp plant is an annual plant that reaches a height of about 2 to 2.5 meters at maturity and the diameter varies in thickness from 5 to 20 millimeters. The diameter can vary depending on the location, growth per hectare and based on how seeds are sown. The hemp bast fibre, used for papermaking can have fibre length from 5 to 55

millimeters. The diameter can vary between 0.016 and 0.050 millimeters. The fibre is distinguished by having fork ends. It takes between 80 to 150 days to mature for fibre harvesting. It is very critical that the hemp is harvested in proper time to satisfy fibre quality [1]. Early or delayed harvesting is done to get fibre quality required for specific application. Hemp is harvested in pre-flowering stage to get fibres for textile manufacturing. In pre-flowering stage, hemp plant gives more bast and fine fibres, which have low lignin content. Hemp harvesting in post seed production stage gives coarse fibres, which are used in composites. Pest and disease resistance of hemp is higher than most of other agricultural crops. It can be grown in most parts of the world without any use of pesticides and insecticides.

Canadian government announced licensing of the commercial production of hemp in 1998. Hemp crop in Canada can yield an average of 9 tonnes per hectare of dry matter [2].

Hemp is not currently used on large scale, but due to its special properties use of hemp fibre is increasing every year. Small-scale uses are currency papers, cigarette paper, textiles, composite, insulation and automotive parts.

1.1.2. Flax

Flax is an annual plant, which grows to a height of 0.50 to 1 meter. Flax is an old crop. It has been farmed in North America since 300 years ago. Flax fibre can have fibre length from 16 to 55 millimeters. The diameter can vary from 0.014 to 0.028 millimeters. Because of the availability of cheaper synthetic fibres, cultivation of fibre flax in North

America was discontinued in the mid-1950. Only oilseed flax is grown in North America today.

Prairie Provinces of Canada are world's largest producer and exporter of flaxseed. Oilseed flax is harvested normally in late summer /early fall. Over 800,000 hectares of flax is grown annually on the prairies. About 500,000 to 1 million tonnes of straw are produced annually [3].

Currently most of the flax straw is burned or chopped and spread. Schweitzer-Mauduit Canada Inc. (SMI) annually processes about 80-120,000 tonnes of flax straw for cigarette paper. Other small-scale uses are plastic composites, specialty paper, paper recycling (fibre) and animal bedding (shives) [3].

1.2. Non-wood Plant Fibre Characteristics

There is considerable variability within particular species of non-wood plant fibre raw material. Unlike wood, which takes years to grow to pulpwood size, most commonly used non-wood plant fibre sources are annual plants and the entire plant develops within relatively short growing period. Plant genus, climate, soil conditions and farming practices all have a large impact on the plants and ultimate pulp fibres [4].

Table 1-1. Physical characteristics of common fibres

Fibre Source	Length (mm)			Diameter (mm)			L/D Ratio
	Max	Min	Average	Max	Min	Average	
Bast Fibres							
Industrial Hemp	55	5	20	0.05	0.016	0.022	1000:1
Oilseed flax tow	45	1	27	0.03	0.016	0.022	1250:1
Textile flax tow	55	16	28	0.028	0.014	0.021	1350:1
Stalk Fibres							
Sugarcane Bagasse	2.8	0.8	1.7	0.034	0.010	0.02	85:1
Wheat Straw	3.1	0.68	1.5	0.024	0.07	0.013	110:1
Corn	2.8	0.68	1.26	0.02	0.010	0.016	80:1
Woods							
Softwood	3.6	2.7	3	0.043	0.032	0.030	100:1
Hardwood	1.8	1	1.25	0.05	0.020	0.025	50:1
Source: Hurter [4]							

Table 1-2. Chemical characteristics of common fibres

Fibre Source	Cellulose (%)	Lignin (%)	Hemi cellulose (%)	Ash (%)	Silica (%)
Bast Fibres					
Industrial Hemp [1]	57-77	9-13	-----	----	----
Oilseed flax tow	34	23	25	2-5	-----
Textile flax tow	50-68	10-15	6-17	2-5	<1
Stalk Fibres					
Sugarcane Bagasse	32-44	19-24	27-32	1.5-5	0.7-3
Wheat Straw	29-35	16-21	26-32	4-9	3-7
Woods					
Softwood	40-45	26-34	7-14	1	<1
Hardwood	38-49	23-30	19-26	1	<1

Sources:
1. http://www.gov.mb.ca/agriculture/crops/hemp.html
2. Hurter [4]

1.3. Objectives of the Thesis Work

Long and strong hemp bast fibres have caught the eye of papermaking community, which is leading to a renewed interest in research. Bast fibres have the potential to increase the tensile strength and tear strength of paper cost effectively. In today's cost conscious paper industry, this can result in a competitive edge over others manufacturers.

Bast fibres along with their strength and length advantages also bring some processing problems. In order to form paper from fibre suspension, fibre suspension is spread evenly across the width of machine at head box. Smook [5] explained that the function of headbox is to take the stock delivered by a pump and transform the pipeline flow into an even, rectangular discharge equal in width to paper machine and at uniform velocity in the machine direction. Since, the formation and uniformity of the final products are dependent on the even dispersion and proper orientation of fibers, the proper operation of the head box system is absolutely critical to a successful papermaking system.

Hemp bast fibres have the inherent tendency to get hydroentangled which gives rise to flow properties different from wood fibre suspensions. Hydroentangled fibres are hard to distribute uniformly which cause plugging of the headbox and non-uniform paper formation. In order to use hemp bast fibers for papermaking this problem needs to be solved.

The objective of this work is to understand the effects of various process variables on hydroentanglement and orientation of hemp bast fibres. Experiments have been carried out to study the dependence of hydroentanglement on fibre length, consistency and hydrodynamic conditions. Fibre orientation has been also studied using data from these experiments.

1.4.Thesis Layout

This thesis is divided into four main sections

1. Literature Review
2. Experimental Design
3. Results and Discussion
4. Conclusion

The first section gives a brief summary of the previous works conducted to study the various factors affecting the flow of fibre suspension in pipes. The parameters used by various investigators to characterize fibre entanglement and flocculation are also defined in this section. The previous works in the area of fibre orientation study are also mentioned.

The second section deals with the experiments performed in our laboratory to study the hydroentanglement and fibre orientation. This section explains the experimental setup, raw material preparation, data collection and data processing. In data processing, the Intensity method used for studying hydroentanglement of fibres and the Fast Fourier Transform method used for studying fibre orientation are explained.

The third section contains results and discussion. The results are presented as those obtained from pressure drop readings and image analysis. The various reasons for getting specific trends are also discussed in this section.

The last section gives a brief summary and conclusions.

Chapter 2. Literature Review

2.1 Factors affecting the flow of fibre suspensions in pipe

The flow of fibre suspensions depends upon

1. Fibre properties like length, axis ratio, surface properties, interaction of fibres, fibre coarseness and fibre flexibility.
2. Pulp consistency and viscosity.
3. Fibre interaction with fines, coagulants, flocculants and air bubbles.
4. Flow properties like pressure, temperature, turbulence and shear.
5. Pipe surface roughness.

2.1.1. Fibre Properties

Mason [6] studied hydrodynamics of fibre suspensions by studying fibres in shear field between two concentric cylinders rotating in opposite directions. Rigid fibres tend to rotate indefinitely in the same orbit until they collide with another fibre, while flexible fibres undergo complex pattern of continually modifying paths. The rotational motion of rigid cylindrical fibres is governed only by the ratio of the length to diameter (the "axis ratio") and not by actual size.

Mason [7] observed that the interaction of fibres is similar to that of rigid cylinders, but is complicated by bending. At very low consistencies, i.e. less than 0.05% by weight, interactions are very frequent and cause the particles to move in erratic orbits. In many instances when two fibers collide while undergoing flexible rotations, they become entangled around one another and execute a number of rotations before disentangling. It was observed that this entanglement is facilitated by bending of the fibre i.e. is favored

by increased fibre flexibility. At slightly high consistencies, fibre aggregates having a dynamic structure i.e. aggregates which are continuously gaining fibres by collision and losing them by disentanglement, can be separated.

Forgacs and coworkers [8] observed suspending rayon fibres of uniform diameter and various lengths in various shear fields that the flexibility and type of rotation of fibres are functions of length and axis ratio. Short fibres of axis ratio <120 rotated stiffly. Longer fibres (120<axis ratio<240) had springy motion. Fibres with axis ratio above 240 had loop like or complex motion. The period of rotation decreased abruptly with increasing length of fibre around axis ratio of 250. This sudden change in the period of rotating clearly separates the stiff fibres from the longer flexible fibres.

Soszynski and Kerekes [9] carried out studies to see the effect of fiber length and diameter on entanglement of fibres using nylon fibres in water in rotating cylinders. They found that entanglement is affected by axis ratio. At low axis ratio (below 40), flocs don't form by fibre entanglement even at high consistencies. As axis ratio increases, flocs form by fibre entanglement even at low consistencies, but they can be easily dispersed by turbulence. When consistency is increased to the level corresponding to 60 fibres in a sphere of the diameter equal to the fibre length, flocs remain intact. For softwood fibres with average length of 3 mm and average diameter of 0.03 mm, the consistency at which flocs remain intact is 0.9 % by volume.

Coarseness of fibres also affects the tendency of fibres to get entangled. Coarseness varies the number of fibres present at a given consistency, number of fibre contacts and fibre flexibility.

2.1.2. Pulp consistency or concentration of fibres

Wollwage [10] tested the effect of consistency by allowing the pulp suspension to flow through a vertically mounted tube. He observed that with an increase in consistency, the number of fibre - fibre collisions increased. This increases the tendency of floc formation. Mason [7] observed that as the concentration of the suspension is increased, a critical concentration is reached above which fibres cannot undergo unimpeded rotations, as there is insufficient space to move. This leads to the entanglement of fibres and the floc formation.

The critical concentration $C_{o,}$ was expressed in volume percent by the relation

$$C_o = \frac{3}{2}\left(\frac{d}{L}\right)^2 \times 100 \qquad (1)$$

where d = diameter of fibre

L = length of fibre

For flexible fibres, the effective length of the fibre is reduced due to bending by an amount that depends upon the flexibility of the fibre. This reduces C_o.

Pressure drop and friction curves for fibre suspensions have several distinctive features, which depend upon the consistency of fibre suspensions. At low consistencies, fibres tend to align in the direction of flow during laminar flow and move randomly in turbulent flow. At moderate consistencies, fibre networks are formed and finite pressure must be applied before flow begins. When mean velocity is increased the pressure loss per unit length of pipe increases to a maximum value then decreases to minimum and drops below water in turbulent region due to drag reduction. At very high consistencies, pulp is conveyed like solids plugs as fibres absorb most of the water.

2.1.3. Fibre interaction with fines, coagulants, flocculants and air bubbles

Coagulants and flocculants increase the retention of fines and their adsorption on fibres.

Kerekes [11] found that coagulants and flocculants increase the physical bonding between the fibres and increase the fibre network strength.

Chang and Robertson [12] found that the increase in network strength is minor when compared to the effect of fibre flexibility.

2.1.4. Fluid Properties

In order to uniformly distribute the fibres on pulp machine, entanglement of the fibres needed to be avoided. In the paper industry, creating enough turbulence in the headbox prevents fibre entanglement.

Robertson and Mason [13] observed the decrease in floc formation by fibre entanglement in the turbulent flow regime.

Flocs are formed by crowding of fibres, entanglement and remaining in crowded entangled form. In turbulent flow, shear forces are present which tend to promote floc formation and dispersion simultaneously. An increase in degree of turbulence favors floc dispersion.

2.1.5. Pipe surface roughness

It has long been known that in turbulent flow a rough pipe leads to a larger friction factor for a given Reynolds number than a smooth pipe does. If a rough pipe is smoothed, the friction factor is reduced until it become hydraulically smooth. Roughness has no appreciable effect on the friction factor unless roughness is very large.

2.2. Parameters to characterize fibre entanglement and flocculation

Mason [7] observed that as the concentration of the suspension is increased, a critical concentration is reached above which fibres cannot undergo unimpeded rotations, as there is insufficient space to move. This leads to entanglement of fibres and floc formation. Critical concentration was defined, as one in which there was less than one fibre in a volume diameter equal to the length of a single fibre.

Kerekes et al. [14] introduced the concept of crowding factor, N. A crowding factor, N, is defined as the number of fibres in a spherical volume of diameter equal to the length of a fibre. Kerekes and Schell [15] calculated crowding factor, N, from volumetric concentration of fibres, C_v, fibre length, L, and fibre diameter, d, using expression

$$N = \frac{2}{3} C_v \left(\frac{L}{d} \right)^2 \tag{2}$$

In terms of mass consistency, for very low consistencies equation (2) can be expressed as

$$N \approx \frac{5 C_m L^2}{\omega} \tag{3}$$

where C_m: mass consistency, %.

ω : fibre coarseness

Kerekes and Schell [15] showed that for a network of randomly distributed uniform fibres, N is directly related to number of contacts per fibre, n_c. Simplifying for $L/d >> 1$ and then combining with Equation (2), they got

$$N \cong \frac{4\pi n_c^3}{3(n_c - 1)} \tag{4}$$

Simplify with $n_c >> 1$, they get

$$N \cong 4n_c^2 \tag{5}$$

They found when $N<1$, fibres are free to move relative to one another in translation. They occasionally collide and may remain temporarily together. As N increases, more collisions take place through translation and then eventually through rotation. When N is such that $n_c \cong 3,$, fibres on average form a continuous network between the bounding walls of the suspension. Moreover, fibres become constrained in rotation relative to one another through three-point contact. From equation (4), n_c =3,occurs at $N \cong 60$. Since contacts on a given fibre are unlikely to alternate on opposing sides of it, restraint in rotational motion may occur at a higher n_c, for example, n_c= 4 or 5 .

Dodson [16] gave an expression for the expected number of contacts per fiber as

$$n_c = 2\frac{L}{d}C_v \tag{6}$$

where n_c: number of contacts per fibre

From equation (2) and (6), we get

$$n_c = \frac{3Nd}{L} \tag{7}$$

2.3. Fibre Orientation

Ullmar and Norman [17] observed the fibre orientation in a headbox nozzle at low consistency using polyester fibres. Enclosing each fibre in an ellipse and defining the orientation of the big axis as the orientation of the fibre estimated the orientation of fibres. This assumption limited the results to fibres, which were almost straight. They

investigated the effect of the flow rate and nozzle contraction ratio on the fibre orientation. They found that the influence of the velocity on the fibre orientation was small, maybe because of the strong elongation flow that tends to align the fibres at the end of the head box.

Ghassmieh and coworkers [18] used fast Fourier transform to obtain orientation distribution of the polyester fibres for the study of microstructural changes of the nowoven.

Chapter 3. Experimental Section

3.1. Experimental Setup

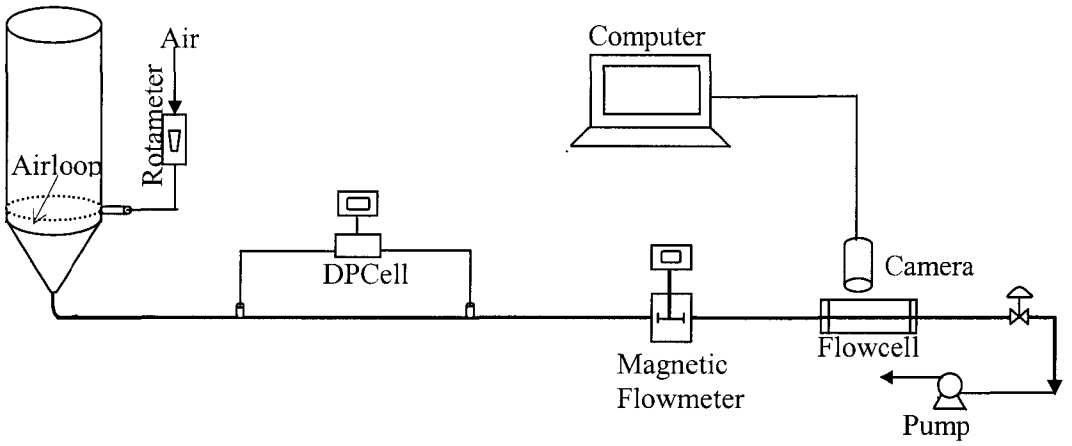

Figure 3-1. Schematic of experimental setup

All experiments were performed on a laboratory –scale flow loop as shown in Figure 3-1. It consists of a 30L feed tank, 1/4" Sch 40 stainless steel pipeline, a DPCell[1], a magnetic flow meter[1], a flowcell and a pump[1]. The setup allowed the fiber slurry flow rate to be controlled using variable- speed drive progressive cavity suction pump[1]. The airflow rate was measured and controlled using a rotameter. The fiber slurry flow rate was measured with a magnetic flowmeter[1]. The pressure drop was measured using a high accuracy DPCell[1] connected to two pressure taps 1.5 m apart. A flowcell made of glass tube with same ID as pipe was placed in the loop. A glass box of rectangular cross section was fitted over the glass tube. The space between the rectangular box and tube was filled with silicone oil to remove curvature effect of the tube.

[1] Appendix [A]

A high-speed camera[1] connected to a computer was used to capture images of the fibers passing through the flowcell. The images were recorded at the rate of 60 frames per second with an image area of 15 mm × 15 mm. The flowcell was illuminated using a back light[1]. To increase the contrast, light was made to come through a slit of 20mm × 20mm. Image acquisition was done using software "Video Savant[1]".

3.2. Hemp fibre processing

3.2.1. Retting Process

Retting is a bacterial or enzymatic process to remove gums and stem tissues from soft fibres, in the processing of natural fibres. This makes decortification (process of separation of bast fibre from core) easier. There are three different methods that are commonly used for retting. They are water retting, dew retting and snow retting [1].

Water retting was used in fibre extraction from hemp stalk. Hemp stalks were dipped in water for 24hr, so that the bast fibre gets loosened from the stalk. Bast fibres were then removed manually from all plants.

3.2.2. Raw material Preparation

Bast strands were dried for a few days to make them easy to cut. Dry bast strands were then cut into 5 mm, 10 mm, 20 mm and 40 mm length using a paper cutter. Samples containing different length of fibres were than cooked separately.

[1] Appendix [A]

3.2.3. Cooking of Hemp fibre

The fibre samples containing different lengths of fibre were soda cooked in an autoclave at temperature of 170°C for 30 minutes at Alberta Research Council. The cooking liquor was drained out from the cooking baskets. Fibres were then stored in a fridge for later use.

3.2.4. Fibre suspension Preparation

Dilute fibre suspension was prepared in batches of 30 liters in the transparent Plexiglas feed tank. Before preparing suspension, moisture content of the cooked fibres was measured.

The moisture content was determined according to TAPPI standards T 412 om-94 and T264 om-93 for oven dry method. Fibre samples were placed in oven at $105 \pm 2^{\circ}C$ over night. The fibre samples were then allowed to equilibrate in desiccators. Once equilibrated, masses of fibre samples were recorded. The moisture content for each sample is calculated as the percentage of the original weight of the sample, to the nearest 0.1%.

$$\text{Percent moisture content} = \frac{(W_1 - W_2)}{W_1} \times 100$$

where W_1 = initial weight of sample, g

W_2 = dry weight of sample, g

Once moisture content of fibres was known, fibre suspensions of different consistencies were prepared from softwood, 5 mm, 10 mm, 20 mm, 40 mm cut and uncut hemp fibres.

Sparging air bubbles into the feeding tank mixed each fiber suspension. The air was introduced near the bottom of tank using an air loop built around the inner circumference. Airflow rate of 12 liter per minute (SLPM) and air pressure of 7 pound per square inch (psi) was used for various fibre length fibre suspensions of 0.01% and 0.02% consistency to achieve uniform mixing. Airflow rate of 20 SLPM and air pressure of 10 psi was used for 0.045% consistency fibre suspensions to achieve uniform mixing.

Whether fibre suspension was uniformly mixed or not was checked by measuring consistency of fibre suspension. Consistency was tested using 5 test samples collected at five different liquid levels in the mixing tank during flow of suspension.

The consistency of fibre suspension was determined according to TAPPI standards T 240 om-93. The sample was first weighed. After that a previously dried, tared filter paper was placed in the Buchner funnel, moistened with water, then applied suction to the flask and filtered the sample slurry. If the filtrate was cloudy, it was refiltered through the same filter paper until it become clear. Resulting pad and filter paper were then removed and dried in an oven at 105 ± 2^{o}C overnight.

The mass consistency, C_m of the sample is then:

$$C_m = \frac{(w - f)}{g}$$

where w = weight of the moisture –free pad and filter paper, g.

f = weight of the moisture –free filter paper, g.

g = net weight of the original sample, g.

3.3. Data Collection

Ten image files with 500 frames each were acquired for every flow rate using 30L of fiber suspension. To ensure uniform mixing and constant flow rate, five flow rate and five consistency readings were recorded during the entire duration of each run. Five pressure drop readings were also recorded along with flow rate and consistency readings. A background image was also acquired for each of the flow rate. The image size for front and background images was at 15 mm × 15mm with 659(H) × 494(V) pixel resolution. All the images were stored in JPEG format for further processing.

3.4. Data Processing

Each image was cropped to size of 500(H) × 250(V) pixels to remove nonuniform illumination present at edges. Background images were then used to 'level' subsequent image frames recorded in image files for each flow rate. As, CCD (charged couple device) camera is a linear device, to do leveling the correct procedure is to divide the acquired image by its background image [19]. Thus, every image frame acquired for a particular flow rate was divided by a background image acquired for the same flow rate. The image processing was done using MATLAB Image Processing Toolbox.

The work was subdivided into two parts 1) Study of hydroentangled hemp fibre flocs 2) Study of orientation of fibres.

The following methods were used to achieve these objectives

1. Intensity Method
2. Fourier Transform Method

3.4.1. Intensity method

When the fibers are hydroentangled they make the acquired image darker as compared to the images that have uniformly distributed fibers for the same consistency. As a result the mean intensity and standard deviation of image frames containing hydroentangled fibers is different than those with uniformly distributed fibers.

Mean intensity and standard deviation for each of the leveled images was calculated. The difference between the mean intensity and the standard deviation for each image frame was then used to detect hydroentanglement. Mean difference for images with unentangled fibres was removed from the series before plotting. In this way, we are able to detect the image frames with hydroentangled fibres as peaks in the plot. A MATLAB Program[2] was written to implement the intensity method.

In order to validate this method, results were first compared with the acquired image frames manually. Figure 3-2 shows the difference between mean intensity and standard deviation of each of the image frame for 0.01% consistency softwood suspension flowing at Reynolds number of 5100. Here the Reynolds number was calculated using the density and the viscosity of water. Before plotting the difference (mean-std) for each image frame, average value of the difference (mean-std) for image frames containing unentangled fibres was calculated by manually selecting the image frames, which doesn't contain hydroentanglement. The average values of mean intensity and standard deviation for image frames containing unentangled fibres were 0.032 and 0.0286, respectively.

Figure 3-2 shows that a difference (Mean-Std) value for all the image frames is very close to zero. This is because of the absence of hydroentanglement of softwood fibres at 0.01 % consistency for Reynolds number of 5100 as shown in Figure 3-3. The average value of mean intensity and standard deviation for the whole of the image file (containing

5000 frames) was also found close to 0.032 and 0.0286. This behavior was prevailing for all the flow rates because consistencies used in these experiments do not provide enough number of contacts per fibre to cause entanglement of softwood fibres. [2] Appendix [B].

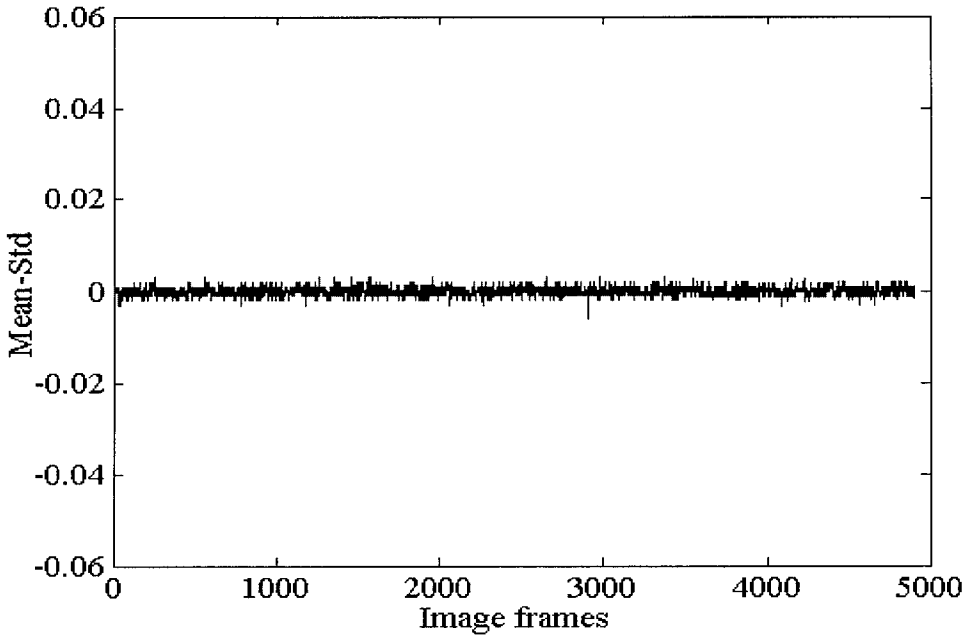

Figure 3-2. Difference vs. Image frames plot for 0.01% softwood fibre suspension

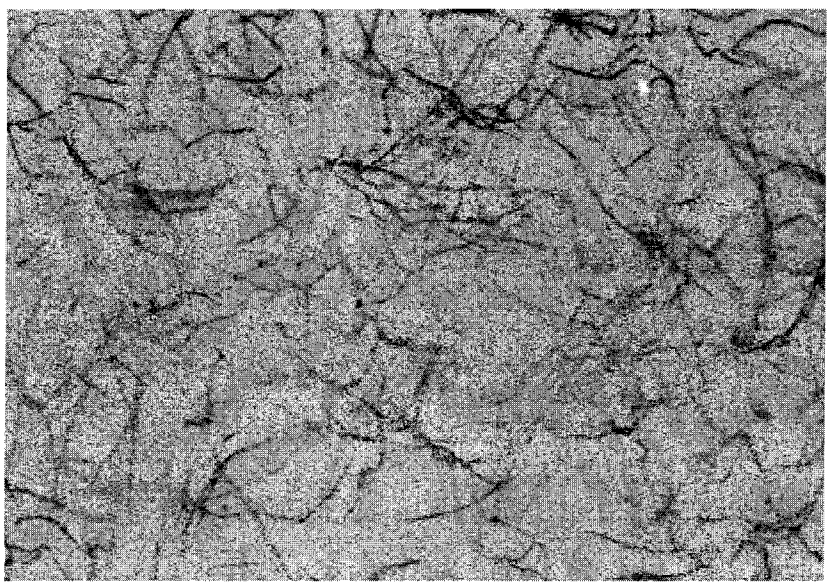

Figure 3-3. 0.01% softwood fibre suspension at Reynolds number of 5100.

Figure 3-4 shows the difference between mean intensity and standard deviation for each of the image frame for 0.01% consistency hemp fibre suspension with fibre length 40 mm and less flowing at a Reynolds number of 5100. Average value of the difference (mean – std) for image frames containing unentangled fibres that was removed from series before plotting was -0.019. The average value of mean intensity and standard deviation for image frames containing unentangled hemp fibres were 0.0032 and 0.0219, respectively. To know what the various peaks in the plot represent, image frames corresponding to various points in the plot were compared manually.

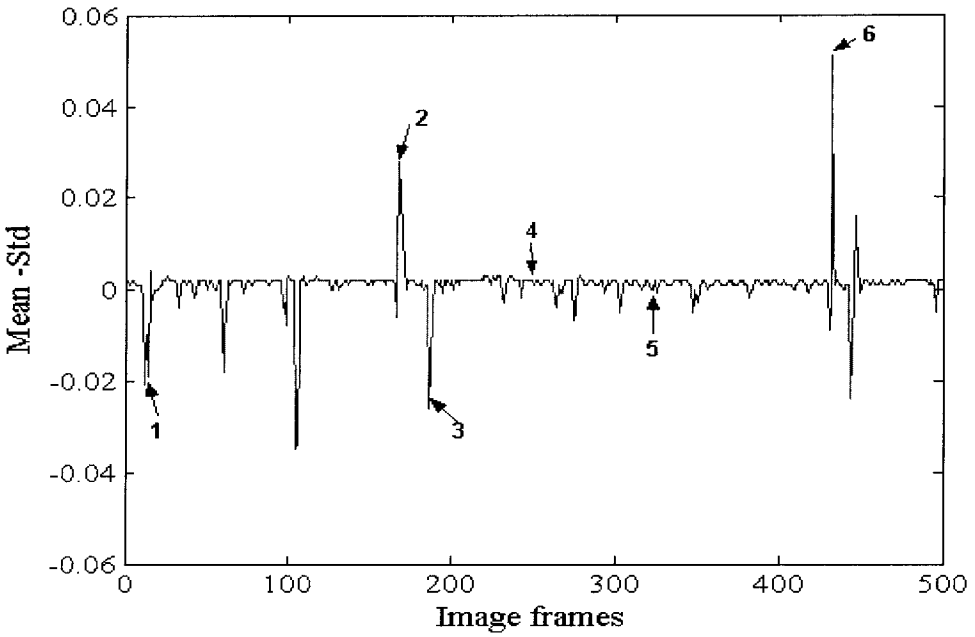

Figure 3-4. Difference vs. Image frames plot for 0.01% hemp fibre suspension.

Figure 3-5 to 3-10, shows the image frames corresponding to point 1 to 6 in Figure 3-4.

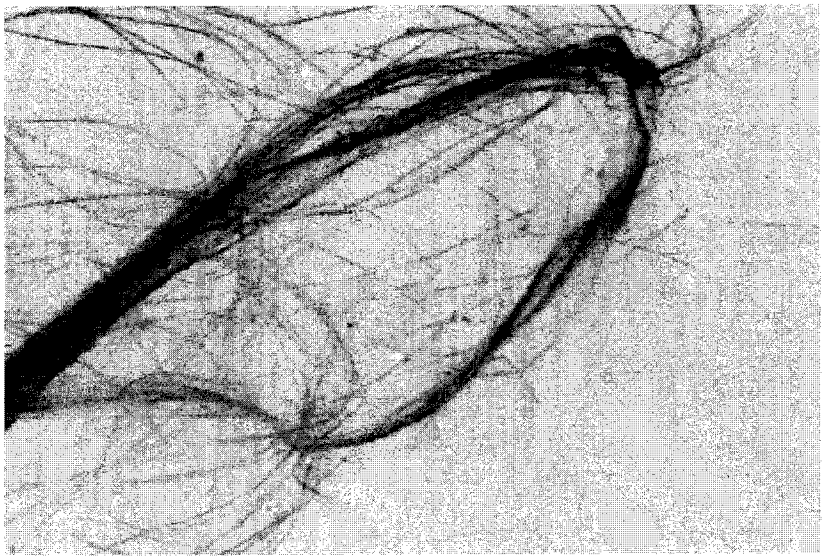

Figure 3-5. Image frame corresponding to point 1 in Figure 3-4.

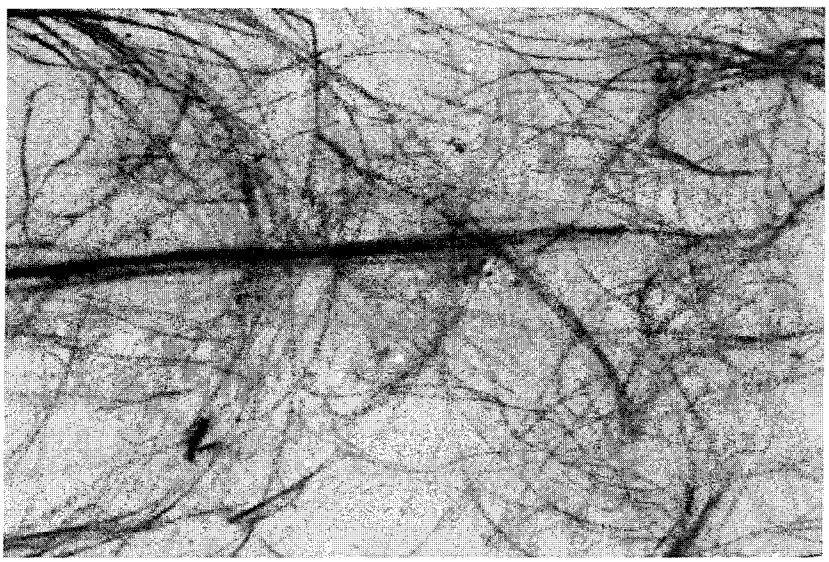

Figure 3-6. Image frame corresponding to point 2 in Figure 3-4.

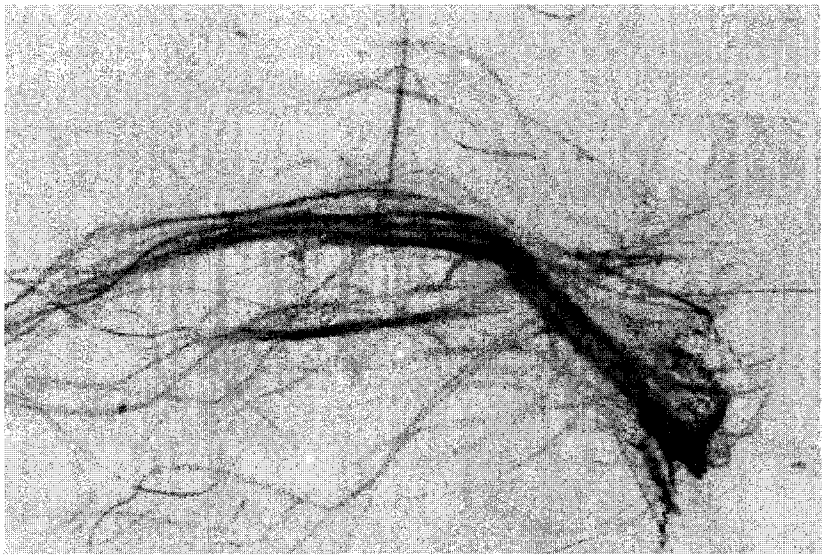

Figure 3-7. Image frame corresponding to point 3 in Figure 3-4.

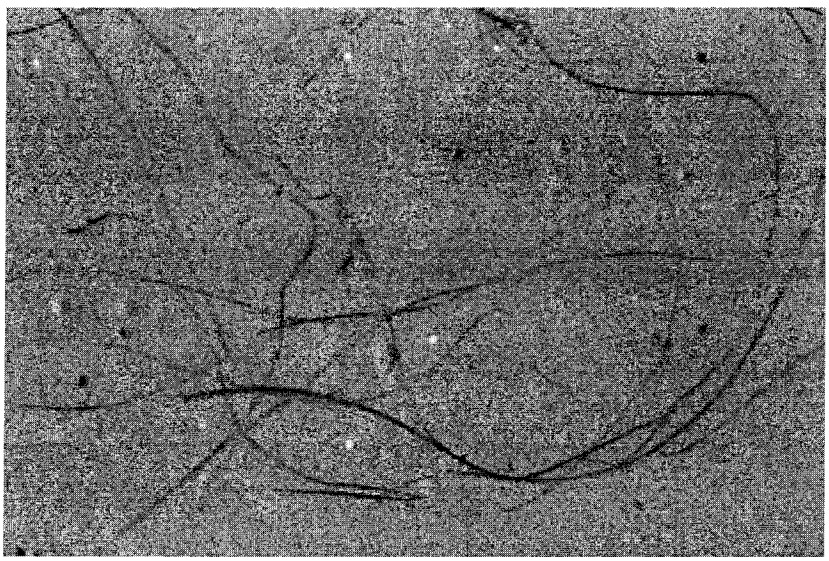

Figure 3-8. Image frame corresponding to point 4 in Figure 3-4.

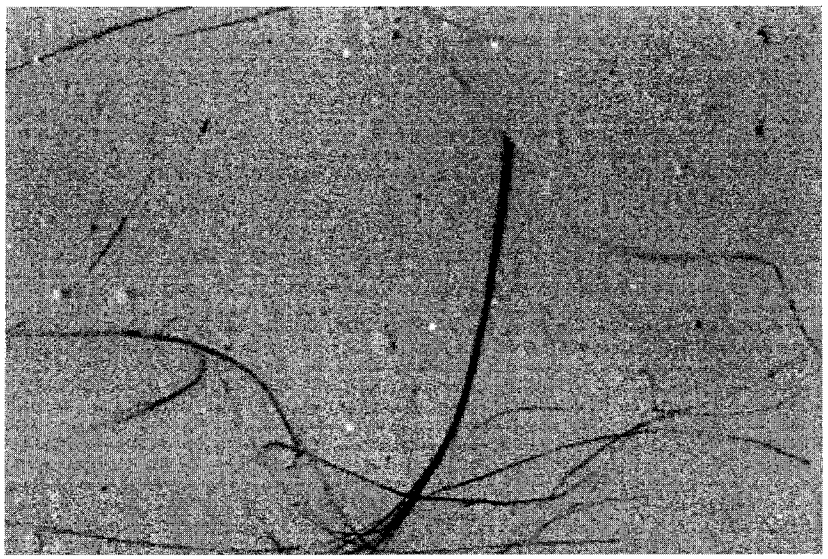

Figure 3-9. Image frame corresponding to point 5 in Figure 3-4.

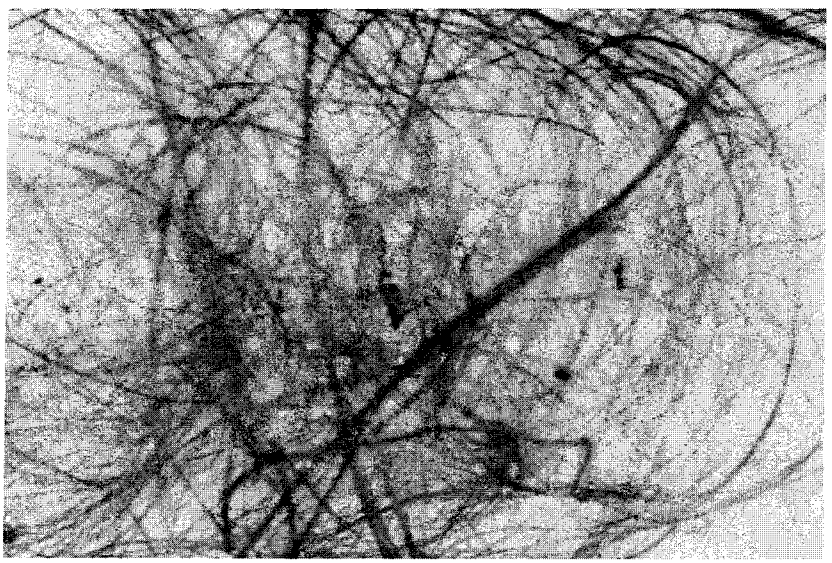

Figure 3-10. Image frame corresponding to point 6 in Figure 3-4.

By comparing Figures 3-5 through 3-10 with their corresponding points in Figure 3-4, it is clear that the lower peaks and upper peaks in Figure 3-3 represent the image frames containing hydroentangled fibres. Lower peaks are caused by flocs of hydroentangled fibres containing thin fibres entangled with thick fibres or strands of bast fibre. High pixel intensity of thick fibres increases the standard deviation of image frame due to which difference (mean-std) becomes negative. Upper peaks are caused by the flocs of thin hydroentangled fibres uniformly covering the whole image frame. These flocs give high mean pixel intensity value and relatively low standard deviation for the image frame, which makes the difference (mean-std) positive. Point 4 and 5 in Figure 3-4, represents Figure 3-8 and 3-9 that contain unentangled fibres. Difference (mean-std) for image frames with un-entangled fibres is around zero.

Therefore, the total number of upper and lower peaks in the Difference (mean-std) vs. Frames plot represents the number of image frames with hydroentangled fibres encountered during the flow.

3.4.2. Fast Fourier Transform (FFT) method

An image is composed of spatial details in the form of brightness transitions. The rate at which these transitions occur is the spatial frequency that is of interest. Spatial frequencies in image containing fibres are related to the orientation of the fibres; fibres are shown in black on a white background. The Fourier transforms are useful in determining the rate at which intensity transition occurs in a given direction in the image. If the fibres are predominantly oriented in a given direction, the spatial frequencies in that direction will be low and the spatial frequencies in the perpendicular direction will be high. This property of the Fourier transform is used to obtain information on fibre orientation distribution [21].

A Fourier transform decomposes an image from its spatial domain of intensities into a frequency domain with appropriate magnitude and phase values. The frequency form of the image is also depicted as an image where the gray scale intensities represent the magnitude of the various frequency components [20].

Fast Fourier transform (FFT) is the common transform technique used in image analysis [20]. Pourdeyhimi and coworkers [21] used Fast Fourier transform to measure fibre orientation in nonwovens.

The Fourier transform is implemented by processing all rows one at a time followed by all columns one at a time. The result is a two- dimensional set of values each having a magnitude and phase. The magnitude values are interesting. They are shown in an image to represent the spatial frequency of the original image. By shifting the Fourier transform results the zero frequency components are shifted to the center of the spectrum. Quadrant one and three are swapped with quadrant two and four. The image magnitude spectrum is

then symmetrical about the center of the image and the center represents the zero frequency. The magnitude of each frequency is indicated by the intensity of the pixel at that location. Since the center of the spectrum contains mostly the noise, the magnitude values of this section are eliminated from subsequent calculations. The fibre orientation can be directly computed from the transform image by selecting an annulus of width *w* at a radius *r* from the center of image and scanning image radially [18].

An average value of the transform intensity is found for each of the angular cells. Since orientation is limited to a range of 0-π, the results are averaged for that range and its radially symmetric counterpart. The width and radius of the annulus influence the results. Another factor that can influence the results from the Fourier transform is the spatial resolution as specified by the number of pixels per unit area [21].

Before calculating Fast Fourier transform of an image, non-uniform illumination at the edges is removed by cropping the image and dividing it by background image. Then, edge detection is conducted.

The edge detection finds local maxima and minima (edges) in the gray scale only. Thus, if the area around a pixel does not undergo large intensity changes over the dimension of the edge detector, the result of applying the edge detector will be close to zero (little or no edge) and lower than the mean gray level for that region. In this case, that pixel is considered to be the background. Otherwise, the result of applying the edge detector is large and pixel is considered to belong to a fiber [21].

In our study, Canny method was used for edge tracking of fibres. The Canny method finds edges by looking for local maxima of the gradient of image. The gradient is calculated using the derivative of a Gaussian filter. The method uses two thresholds, to

detect strong and weak edges, and includes the weak edges in the output only if they are connected to strong edges. The input threshold values were chosen manually by comparing edge tracking image with original image at various threshold values. This method is less likely than the others to be "fooled" by noise, and more likely to detect true weak edges

A MATLAB Program[3] was used to implement Fourier transform method involves dividing the image by its background, edges tracking using Canny's method, Fast Fourier transform calculation, quadrant swapping, selecting an annulus, slicing annulus into 10 degrees cells and computing average transform intensity in each cell.

Figure 3-11 shows a sample image of stationary hemp fibre bundles. The edge thesholded image of Figure 3-11 using Canny's method is shown as Figure 3-12. Figure.3-13 illustrates the fibre orientation distribution obtained from Fast Fourier Transform of sample image. Since orientation was limited to a range of 0-π, normalized transform intensity was calculated as

$$NTI = \frac{\pi \times TI}{\int_0^{\pi} TI d\theta}$$

where NTI = Normalized Transform intensity

TI = Transform Intensity

[3] Appendix [C]

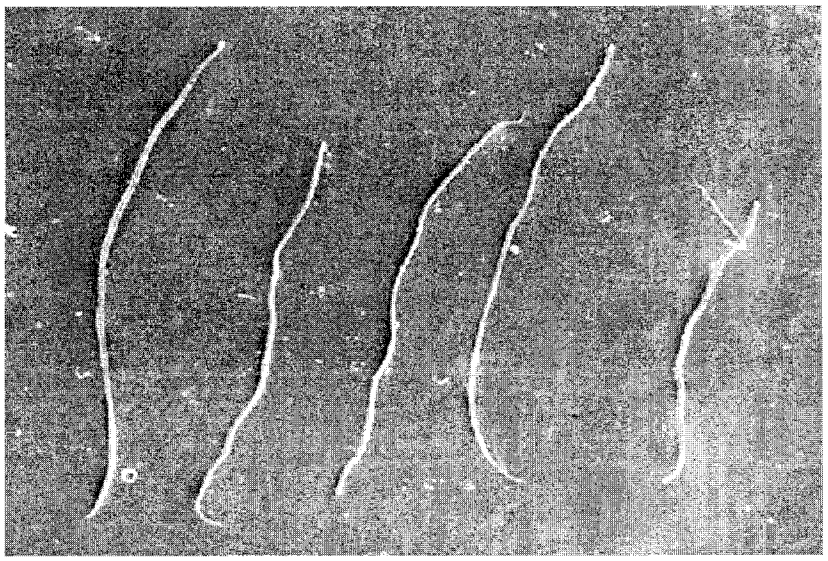

Figure 3-11. Sample image of hemp fibre bundles.

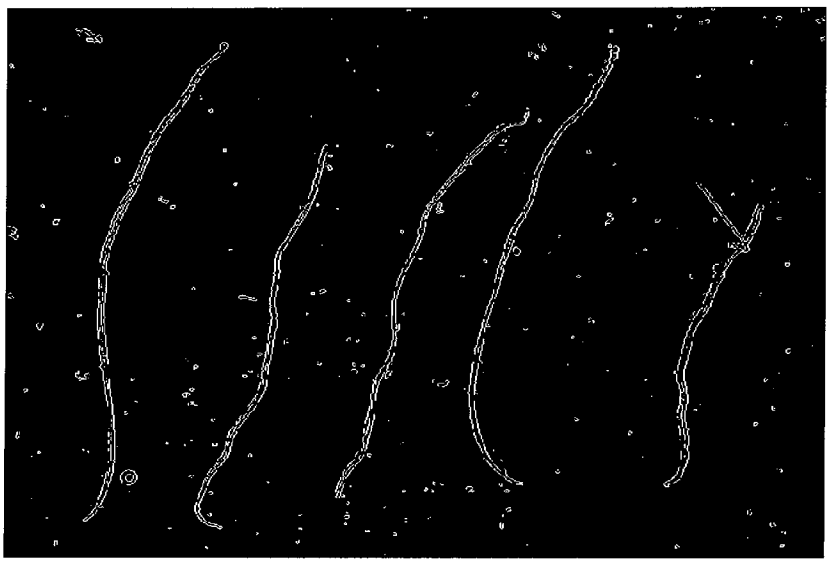

Figure 3-12. Edge threshold image of sample image.

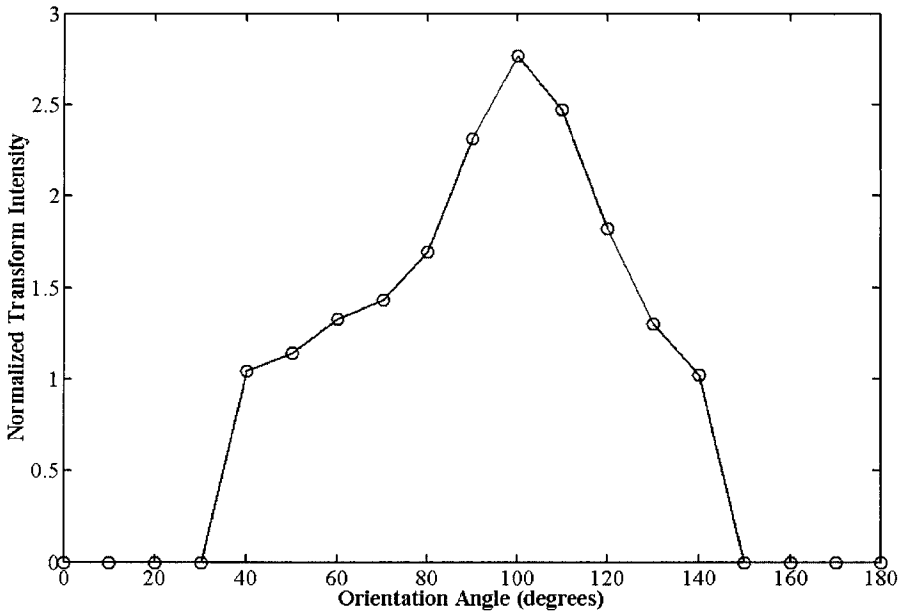

Figure 3-13. Fibre orientation distribution of sample image.

Figure 3-13 shows that maximum normalized transform intensity corresponds to the orientation angle of 100°. This means that most of the fibres are orientated at 100°. The visual inspection of the sample image confirms the result. This confirms that the MATLAB program used to implement the Fourier transform method is giving accurate results.

Chapter 4. Results and Discussion

The objective of this work was to study the hydroentanglement and fibre orientation of the hemp fibres.

In order to understand hydroentanglement and fibre orientation of the hemp fibres, effects of three parameters fibre length, fibre suspension consistency and flow rate were studied on flowing hemp fibre slurry. Pressure drop, fibre suspension consistency, flow rate and image frames were recorded for different flow runs to study their effects.

Friction factor values were calculated from pressure drop readings and results were then plotted to understand the effect of different process variables on friction factor values. Images were analyzed by the Intensity method to calculate the hydroentanglement instances and severity. The Fast Fourier Transform (FFT) method was used to analyze the images to calculate fibre orientation.

4.1. Pressure Drop

Figure 4-1 and 4-2 show friction factor vs. Reynolds number plots for different fibre lengths at various flow rates for 0.01% and 0.02 % consistency, respectively. Friction factor was calculated based on

$$f = \frac{(-\Delta p).D}{2\Delta L.\rho.V^2}$$

where f = friction factor

$-\Delta p$ = Pressure drop

D = Diameter of pipe, 9 mm.

ΔL = Length of pipe between pressure taps, 1.5m.

ρ = Density of water at 20°C

V = Average velocity

Reynolds number was calculated using expression

$$\mathrm{Re} = \frac{DV\rho}{\mu}$$

Density, ρ and viscosity, μ of water (suspending fluid) were used to calculate Reynolds number as consistency of fibre suspension was very low.

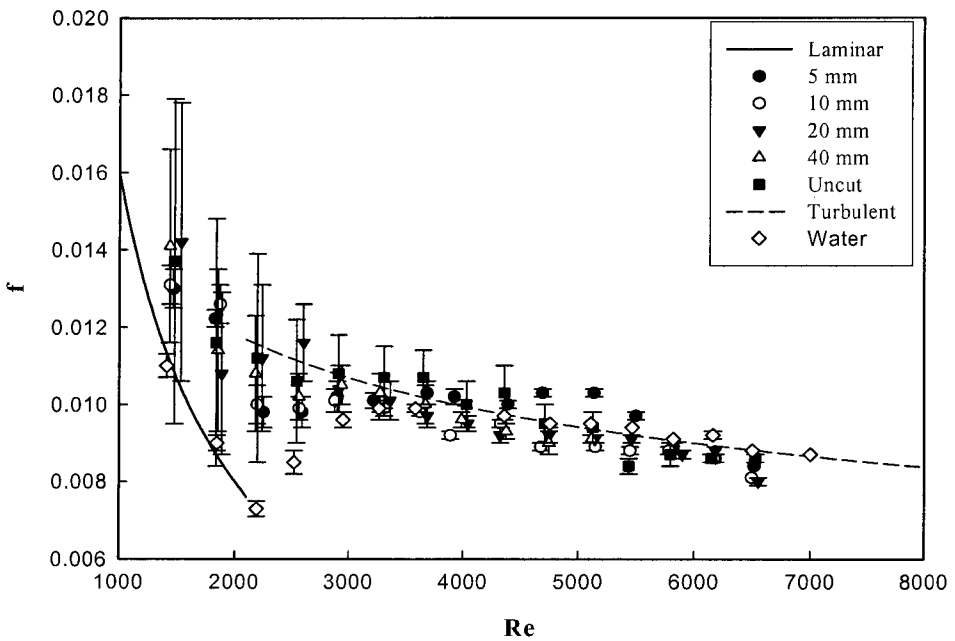

Figure 4-1. Effect of fibre length on friction factor for 0.01% fibre suspension.

One can observe from Figure 4.1 and Figure 4.2 that the friction losses for hemp fibre suspensions are significantly higher than water in the laminar flow regime. In the turbulent flow regime, the friction losses for long fibre suspension are lower than that for water.

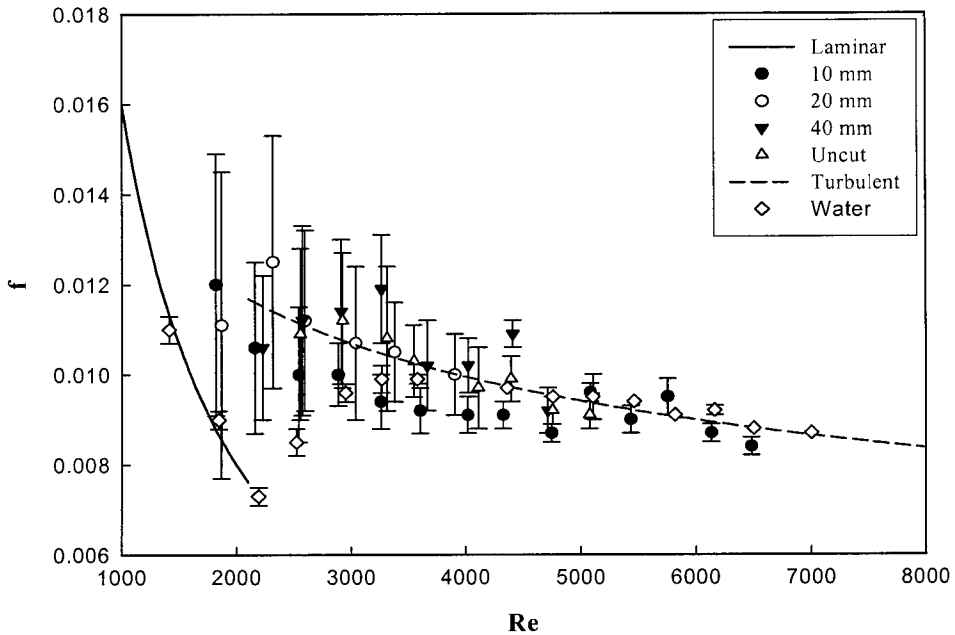

Figure 4-2. Effect of fibre length on friction factor for 0.02% fibre suspension.

Error bars in Figure 4-1 and Figure 4-2 illustrate the variation in friction factor due to fluctuation in pressure drop readings. There is more variation in friction factor at low Reynolds number as compared to high Reynolds number for all fibre lengths. The fluctuation in friction losses can be attributed to the hydroentanglment. As fibre flocs flow by, the pressure drop increases. Presence of fibre flocs also increases the fluctuation in pressure drop readings. In turbulent flow regime, fibres reduce the drag between the pipe wall and the flowing stream, which lowers the pressure drop below that of water. Turbulent flow also breaks fibre flocs, which reduce the fluctuation in pressure drop readings.

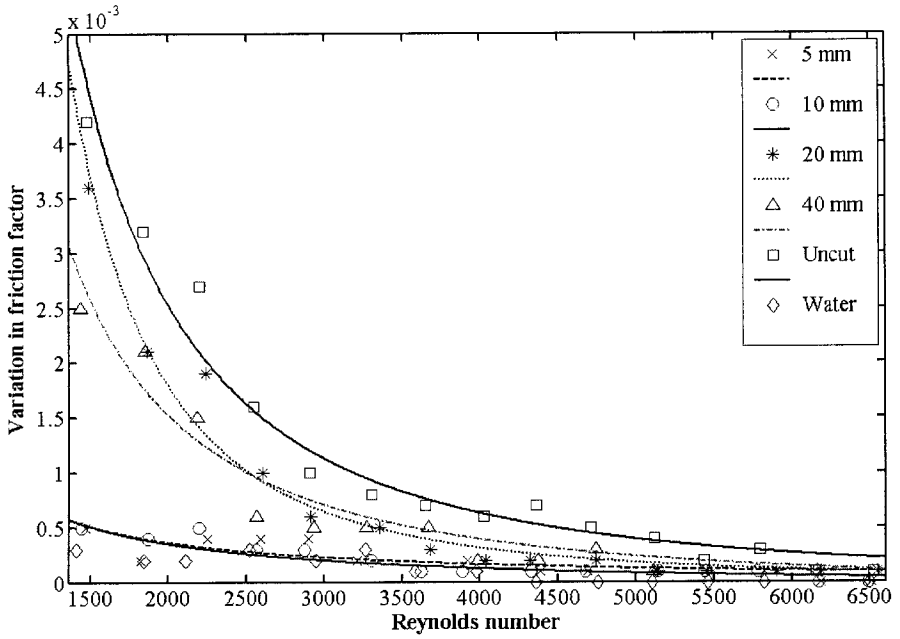

Figure 4-3. Variation in friction factor for 0.01% fibre suspension.

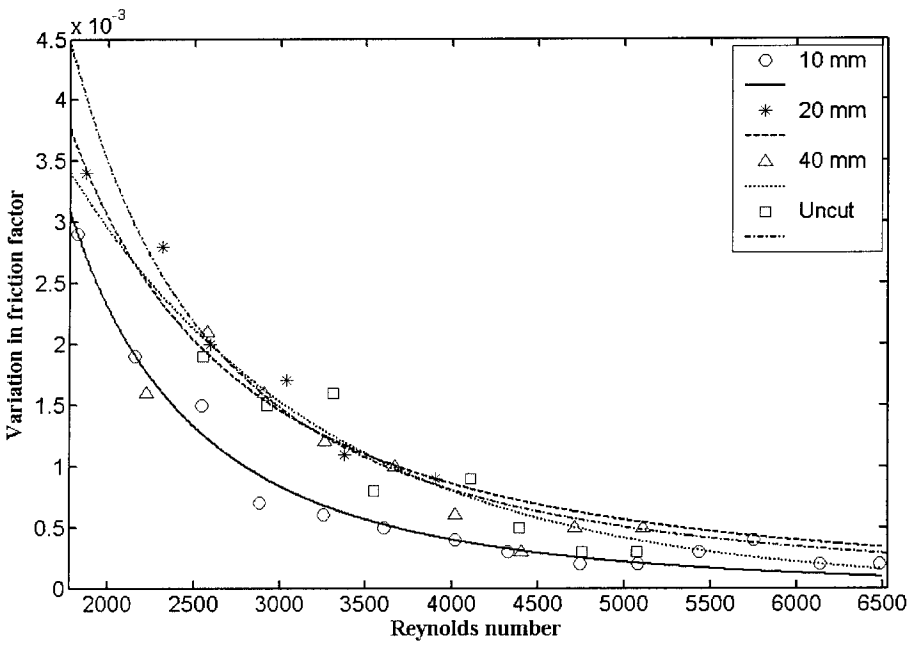

Figure 4-4. Variation in friction factor for 0.02% fibre suspension.

Figure 4-3 and Figure 4-4 show that for both 0.01% and 0.02% consistencies, there is greater variation in friction factor for hemp fibre suspension with longer fibres (i.e. above average length of 1 cm) at low flow rates. Variation in friction factor subsides with increase in flow rate for all fibre lengths.

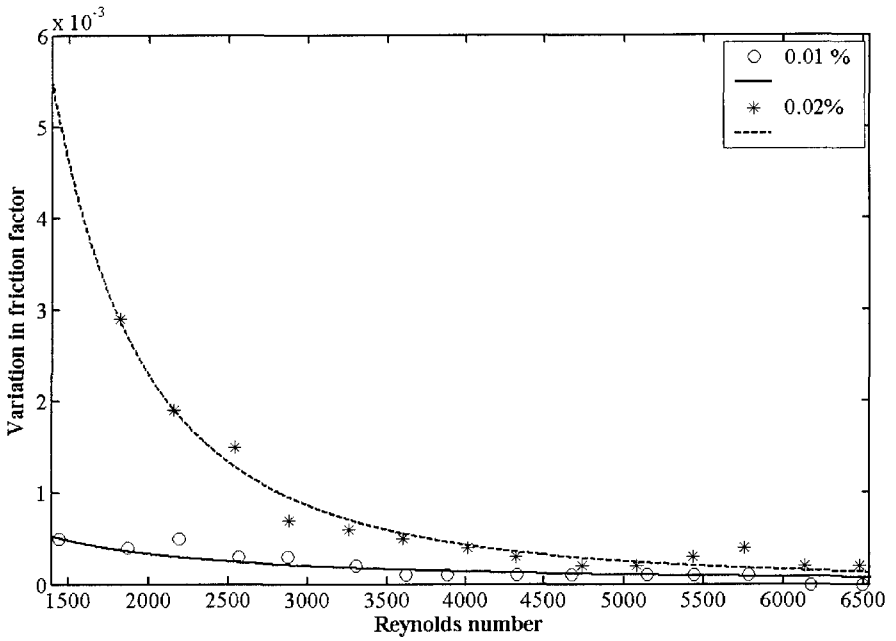

Figure 4-5. Effect of consistency on variation in friction factor for 10 mm cut hemp fibres

Figure 4-5 shows the variation in friction factor for hemp fibre suspension with uppermost fibre length of 10 mm at 0.01% and 0.02% consistency. Variation in friction factor is greater for 0.02% consistency as compared to 0.01% consistency. This can be attributed to the presence of more fibres in the pipe at higher consistency. The higher is the number of fibres present more is the fibre entanglement. For Reynolds number greater than 5500, variation in friction factor for both consistencies tends to become almost similar. This may be due to disentanglement of fibres by turbulence.

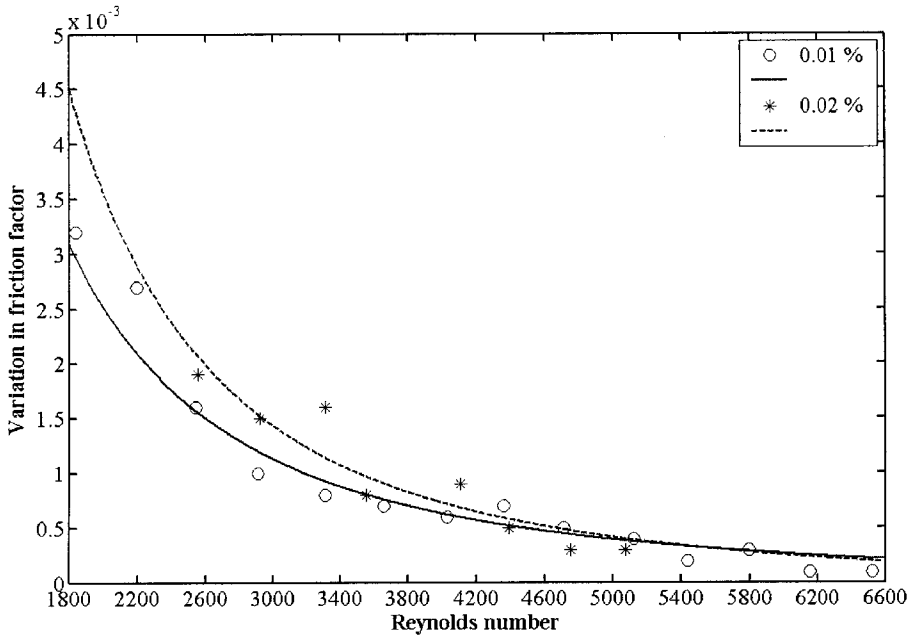

Figure 4-6. Effect of consistency on variation in friction factor for uncut hemp

Figure 4-6 shows variation in friction factor for fibre suspension containing uncut hemp fibres at 0.01% and 0.02% consistency. Figure 4-6 is similar to Figure 4-5 as for both variation in friction factor is greater for 0.02% consistency as compared to 0.01% and variation in friction factor for both consistencies becomes almost similar for Reynolds number greater than 5500. Thus, this behavior can also be explained in a similar manner.

4.2. Intensity method

Figure 4-7 and Figure 4-8 show hydroentanglement instances per unit mass for 0.01% and 0.02% consistency hemp fibre suspension, respectively. It is clear from Figure 4-7 and Figure 4-8, that for both 0.01% and 0.02% consistency hydroentanglement instances per unit mass decrease with increase in flow rate for all fibre lengths. Fibre samples with 20 mm, 40 mm and uncut fibres tend to have approximately the same number of peaks per unit mass. This may be because average fibre length of fibre samples containing 40 mm and uncut fibres is also around 20 mm. Hydroentanglement instances per unit mass increase with decrease in fibre length up to the fibre length of 10mm after which the trend reverses. Fibre samples with 5 mm long fibre show lesser number of hydroentanglement instances per unit mass as compared to that with uppermost fibre length of 10 mm. This may be due to presence of insufficient number of fibre contacts for 5 mm long fibres to get entangled at these low consistencies.

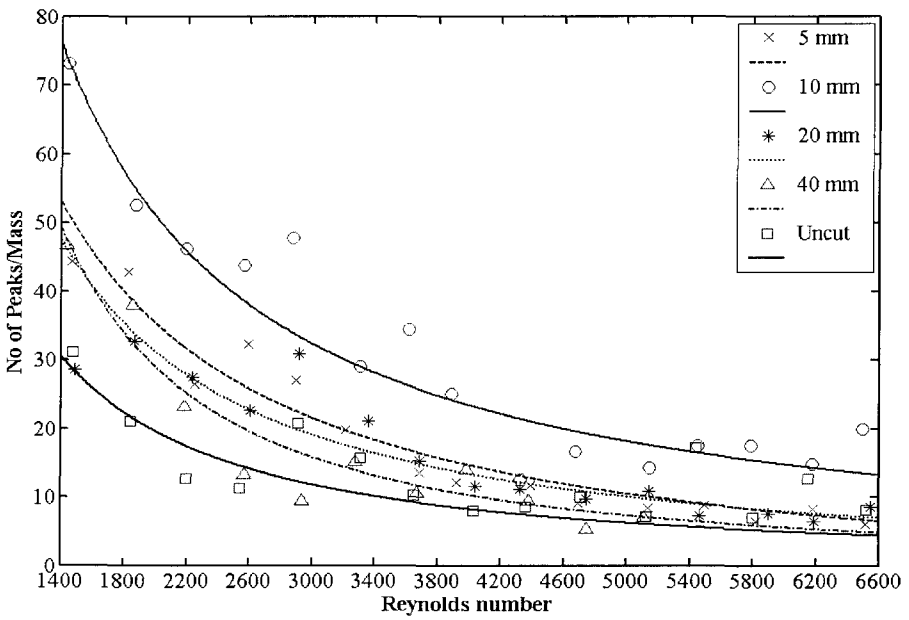

Figure 4-7. Hydroentanglement instances per unit mass for 0.01% hemp fibre suspension.

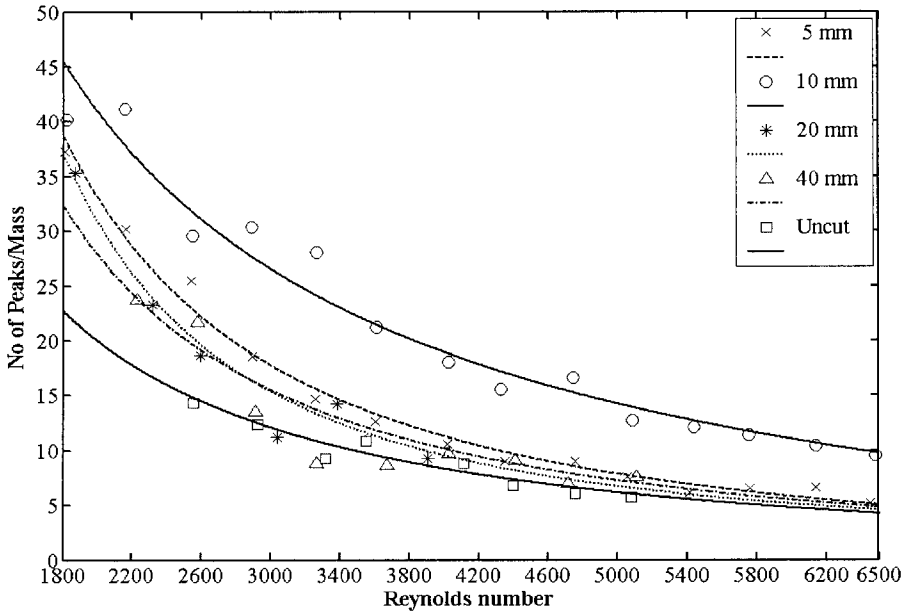

Figure 4-8. Hydroentanglement instances per unit mass for 0.02% hemp fibre suspension.

Figure 4-9 and Figure 4-10 shows that hydroentanglement instances per unit volume increase with increase in consistency. This is due to an increase in the number of fibres per unit volume with increase in consistency. This can also be explained using the expression for crowding factor and number of contacts per unit fibre.

Kerekes and Schell [15], express crowding factor as

$$N \approx \frac{5C_m L^2}{\delta} \tag{3}$$

Dodson [16], gave an expression for the expected number of contacts per fibre as

$$n_{conatcts} = 2\frac{L}{d}C_v \approx \frac{\pi}{2}\cdot\frac{w.L}{\delta}\cdot C_m \tag{6}$$

The above expressions show that the crowding factor and the number of contacts per fibre are directly proportional to the consistency and the fibre length.

An increase in consistency at constant fibre length increases crowding factor and number of contacts per fibre. Increasing the number of contacts increases the chances of fibre entanglement in fibre suspension. This explains Figure 4-9 and Figure 4-10, which show an increase in hydroentanglement instances with an increase in consistency for the same longest fibre length present in fibre suspension. However, an increase in the number of hydroentangled fibre flocs is not according to the relationship given in equation (3) and (6).

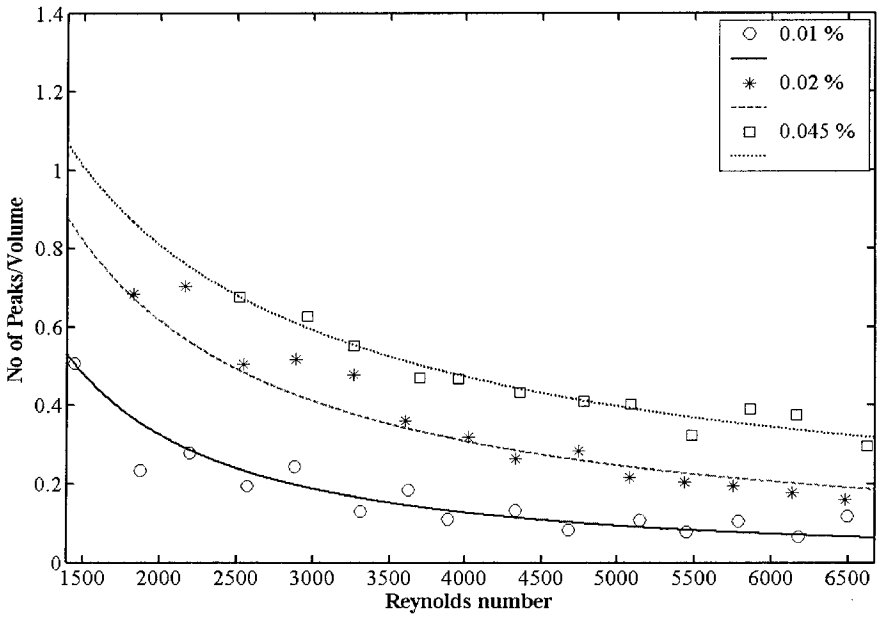

Figure 4-9. Hydroentanglement instances per unit volume for hemp fibre suspension with longest fibre length of 10 mm.

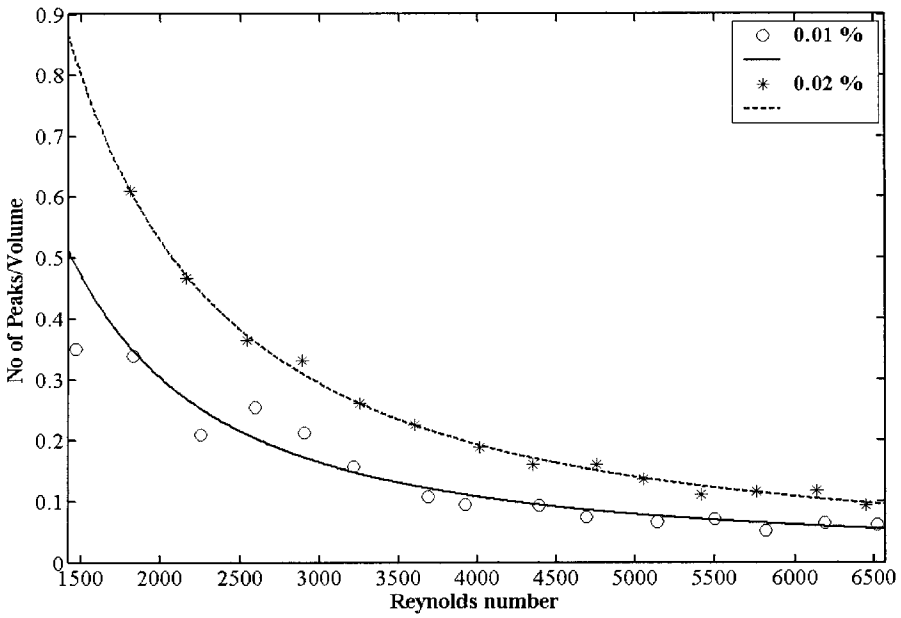

Figure 4-10. Hydroentanglement instances per unit volume for hemp fibre suspension with longest fibre length of 5 mm.

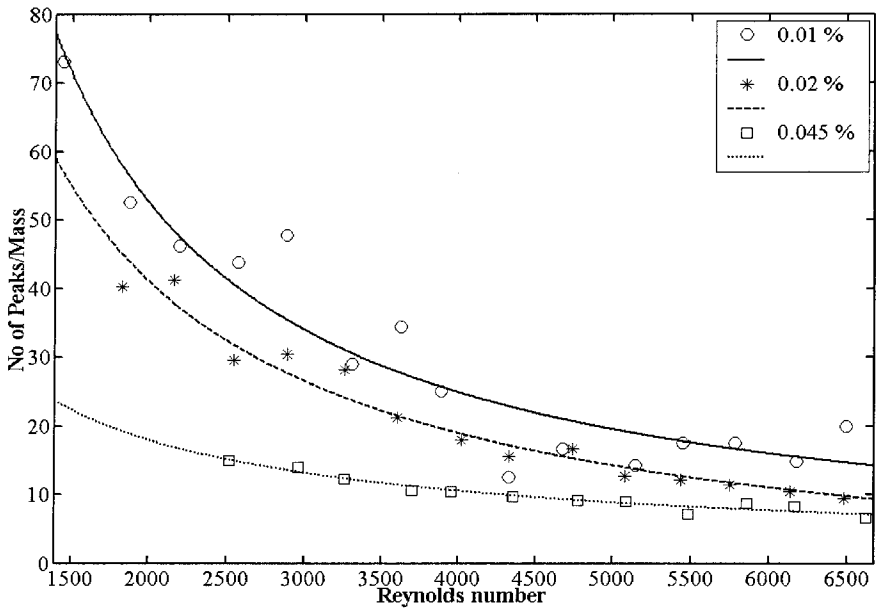

Figure 4-11. Hydroentanglement instances per unit mass for hemp fibre suspension with longest fibre length of 10 mm

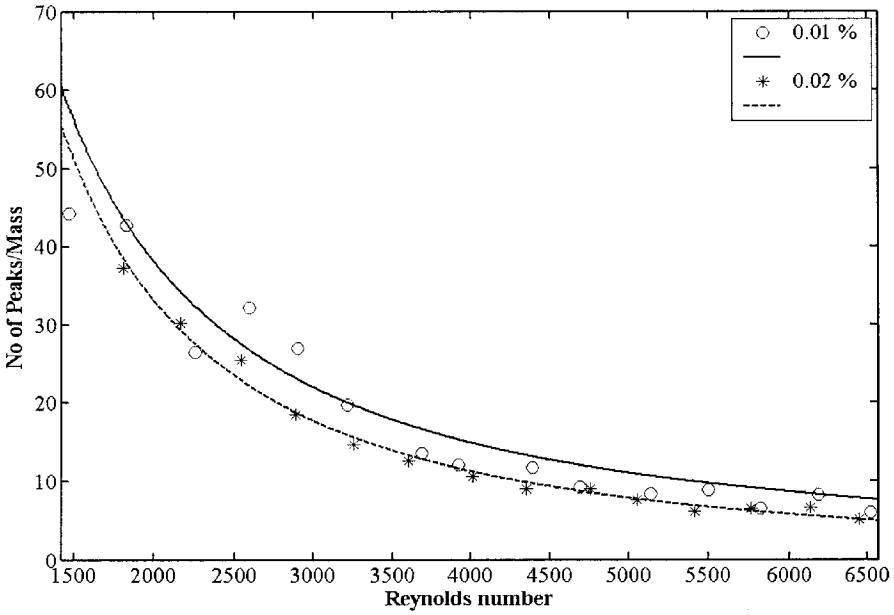

Figure 4-12. Hydroentanglement instances per unit mass for hemp fibre suspension with longest fibre length of 5 mm.

Figure 4-11 and Figure 4-12 show decrease in hydro entanglement per unit mass with increase in consistency for the average fibre length of 10 mm and 5 mm, respectively. This cannot be explained using crowding factor and number of contacts per fibre as according to equations (3) and (6) both curves in Figure 4-11 and Figure 4-12 should collapse into one.

In order to explain Figures 4-7, 4-8, 4-11 and 4-12, the maximum height of upper peaks was measured for all flow rates, which represent the biggest hydro entangled fibre floc present. Figure 4-13 and Figure 4-14 show that maximum height of peaks or the size of the biggest hydroentangled fibre floc present increases with increase in consistency and longest fibre length present in fibre suspension. Thus, increase in consistency not only increases the number of hydroentangled fibre flocs, but their sizes as well.

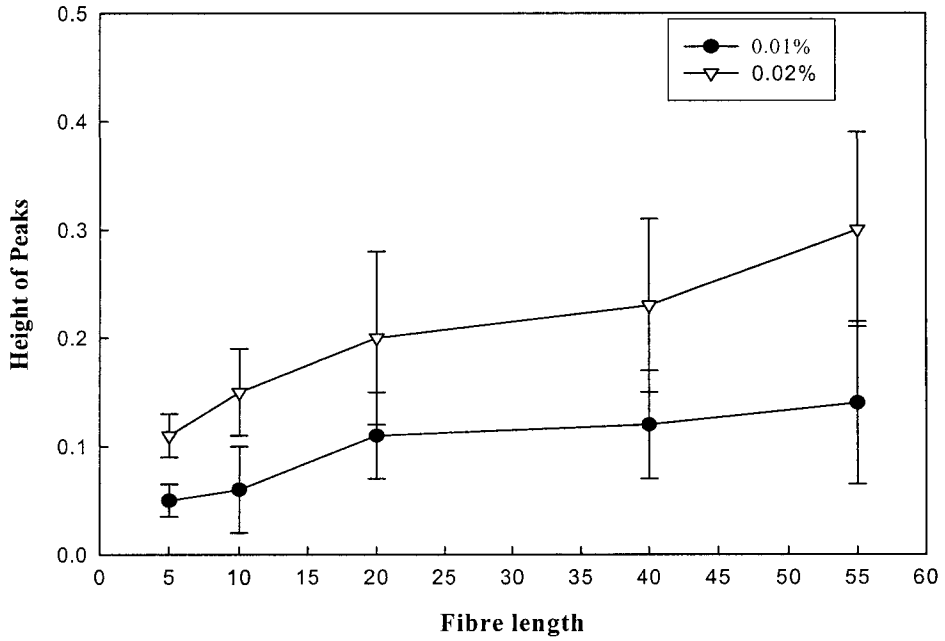

Figure 4-13. Size of hydroentangled fibre flocs for different fibre length.

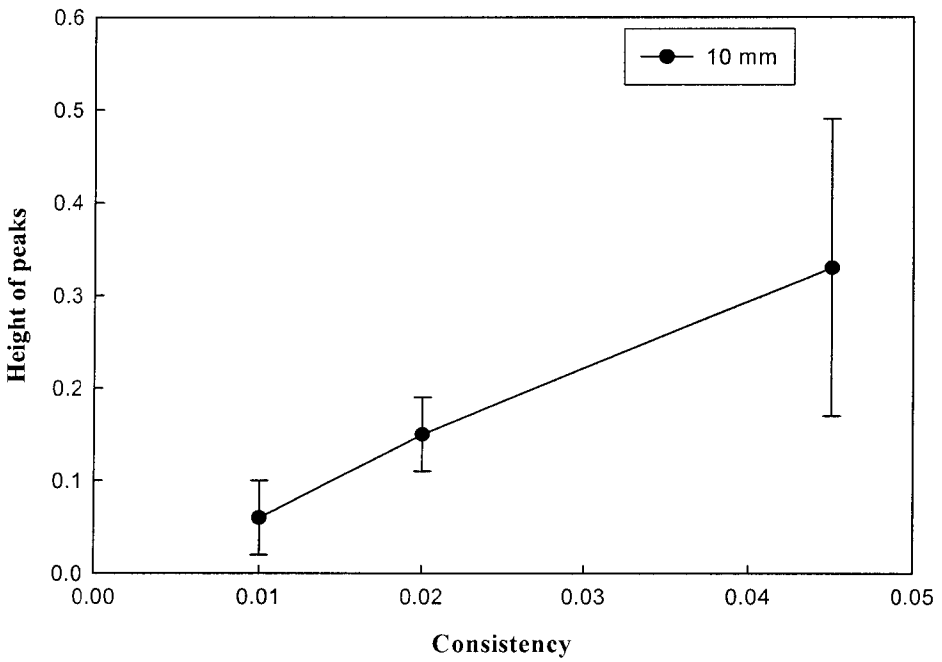

Figure 4-14. Size of hydroentangled fibre flocs for fibre suspensions with longest fibre length of 10 mm at different consistencies.

The hydroentanglement instances per unit mass decrease with an increase in consistency as shown in Figure 4-11 and Figure 4-12 because of the increase in size of hydroentangled fibre flocs.

Figure 4-7 and Figure 4-8 show increases in hydroentanglement instances per unit mass up to 10 mm longest fibre length present in fibre suspension. This is due to decrease in the size of hydroentangled fibre flocs and increase in their number. However, as the fibres are cut to fibre length of 5 mm both the number and size of hydroentangled fibre flocs decreases. This leads to the reversal of the trend.

4.3. Fourier method

Figure 4-15 shows fibre orientation distribution for 0.01% consistency softwood fibre suspension. For laminar flow i.e. Reynolds number of 1500, most of the fibres are aligned at 0 or 180 degrees i.e. along the direction of flow. The probability of fibres aligning perpendicular to the flow direction i.e. 90 degree is minimal. An increase in Reynolds number, tend to make the orientation distribution curve flatter or have fibres more evenly distributed at different angles. This is because higher flow rate involve higher turbulence, which results in more random fibre orientation.

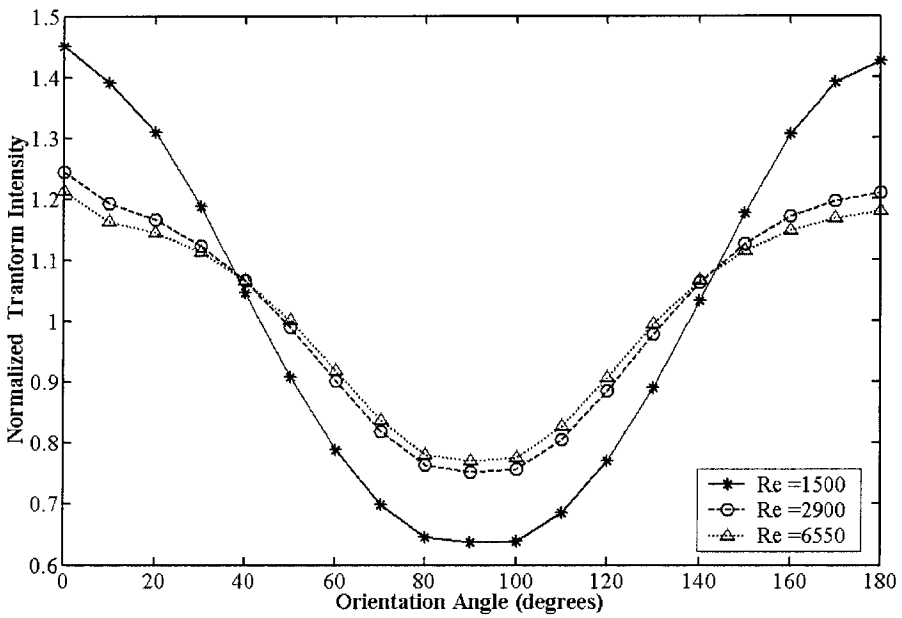

Figure 4-15. Fibre orientation distribution of softwood fibres

Figure 4-16 illustrates the standard deviation corresponding to each point in Figure 4-15. Standard deviation increases with increase in flow rate, which again could be the result of increase in random orientation of fibres due to increase in turbulence.

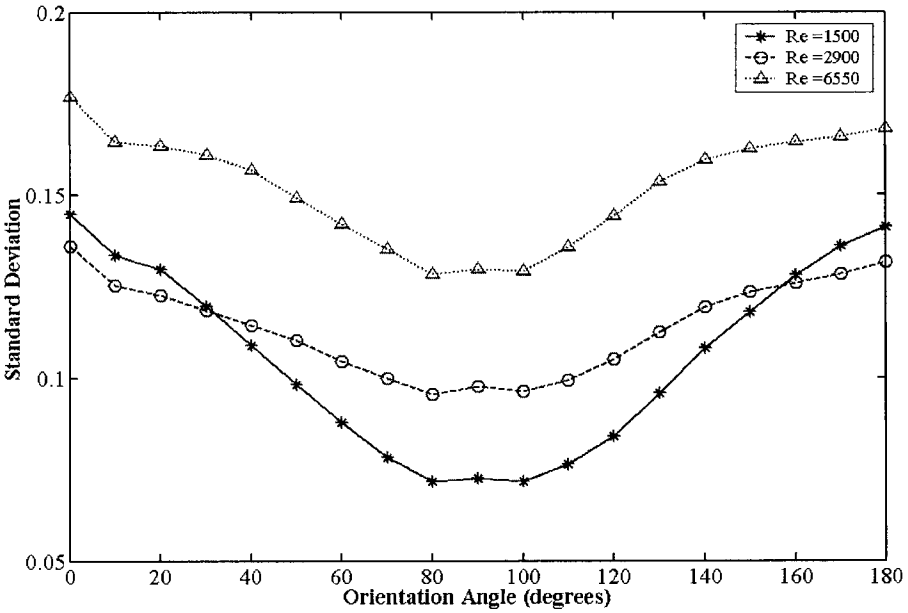

Figure 4-16. Standard deviation for various points in Figure 4-15.

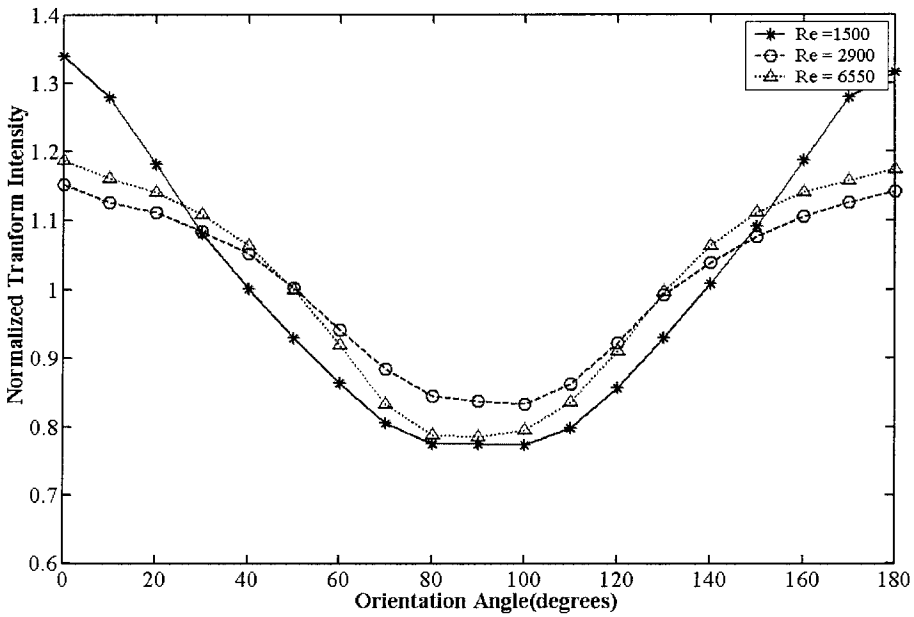

Figure 4-17. Fibre orientation distribution of 5 mm cut hemp fibres

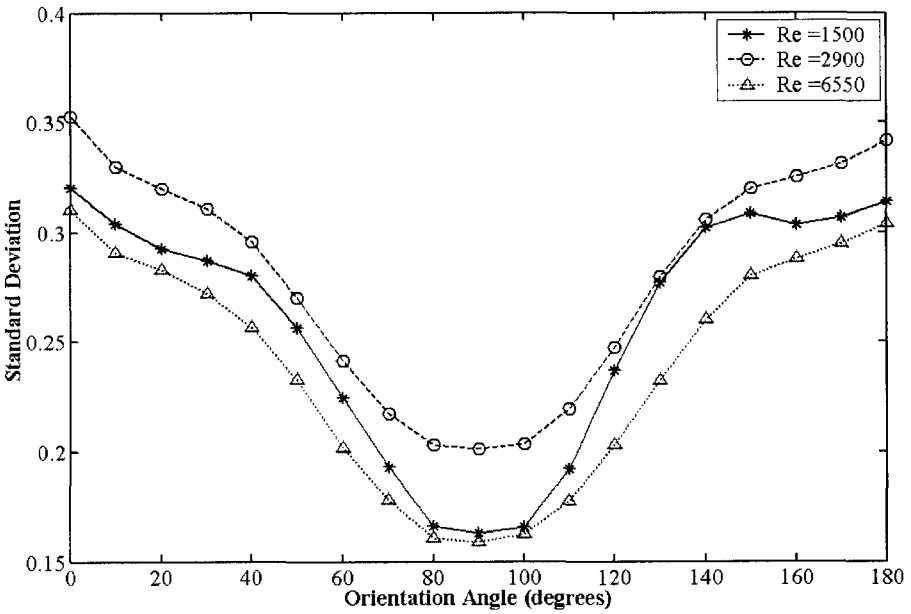

Figure 4-18. Standard deviation for various points in Figure 4-17.

Figure 4-17 shows fibre orientation distribution for 0.01% consistency hemp fibre suspension with hemp fibres cut to 5mm length. Fibre orientation distribution trend in Figure 4-17 is similar to that for softwood fibre orientation distribution shown in Figure 4-15. Figure 4-17 shows more fibres aligned in the direction of flow for laminar flow and greater randomness in fibre orientation for turbulent flow regime.

Figure 4-18, illustrates the standard deviation corresponding to each point in Figure 4-17. Standard deviation for all the points in Figure 4-18 is higher than corresponding points in Figure 4-16. This could be due to hydroentanglement of hemp fibres.

Figure 4-19 shows an image frame of 0.01% hemp fibre suspension with fibres cut to 5 mm length at Reynolds number of 2900. Figure 4-20 shows edge thresholded image of Figure 4-19. Figure 4-22 is the edge thesholded image for Figure 4-21 of hydroentangled hemp fibre of same length and at same flowrate. Comparing Figure 4-20 and Figure 4-22,

it is clear that fibre orientation distribution calculation for image frames with hydro entangled fibres tend to generate erroneous values which increase standard deviation.

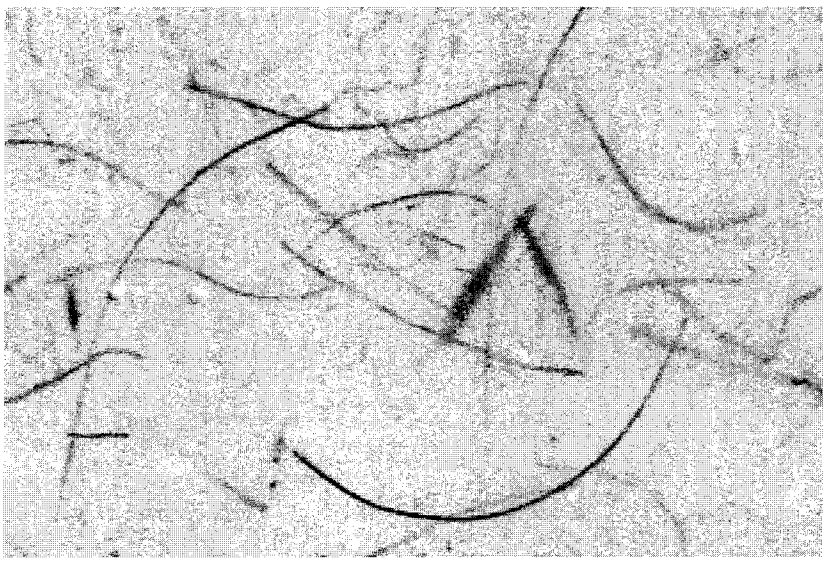

Figure 4-19. Fibre suspension containing 5mm hemp fibres at Reynolds number of 2900.

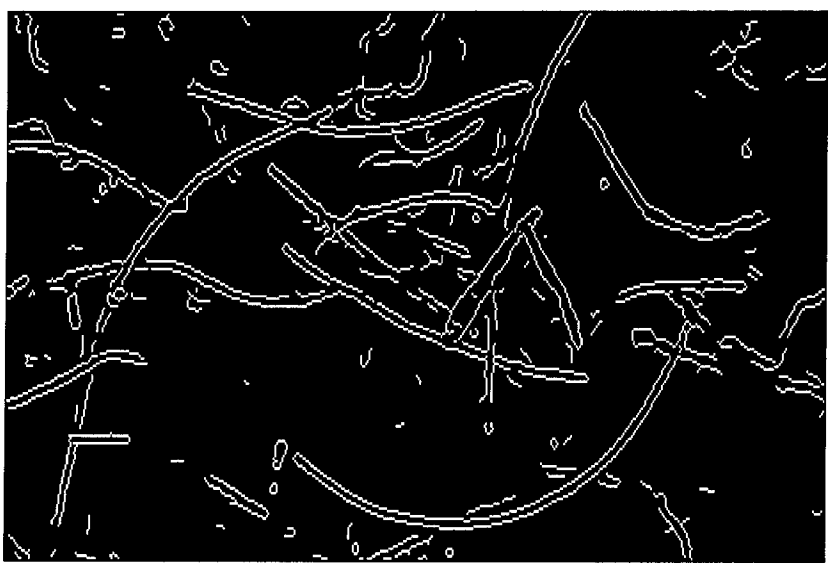

Figure 4-20. Edge thresholded image of Figure 4-19.

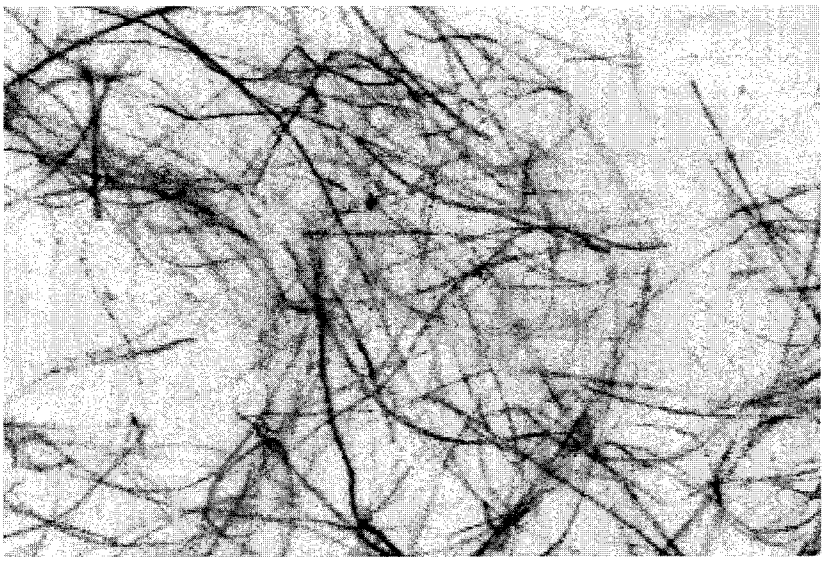

Figure 4-21. Fibre suspension containing (hydroentangled) 5mm hemp fibres at Reynolds number of 2900.

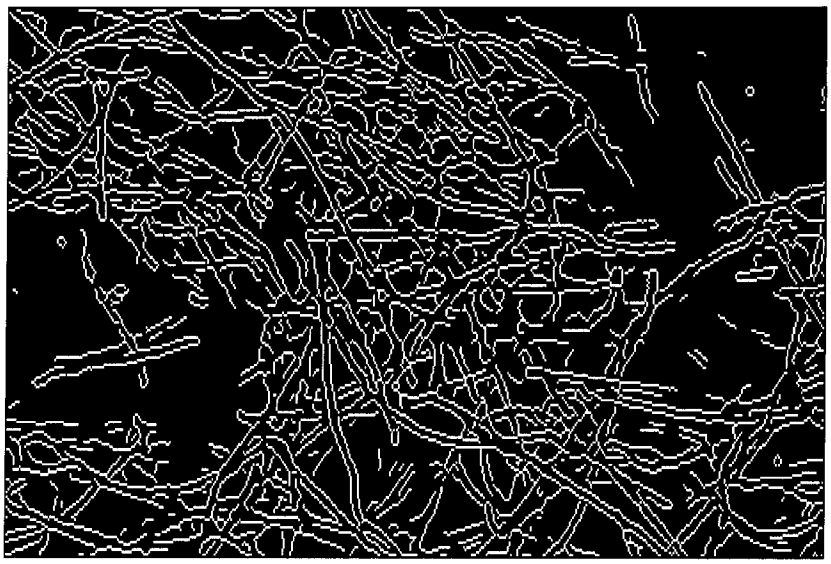

Figure 4-22. Edge thresholded image of Figure 4-21.

Figure 4-23 shows fibre orientation distribution for 0.01% consistency hemp fibre suspension with fibres cut to the length 10mm. Fibre orientation distribution trend in Figure 4-23 is also similar to that for softwood fibre orientation distribution shown in Figure 4-15.

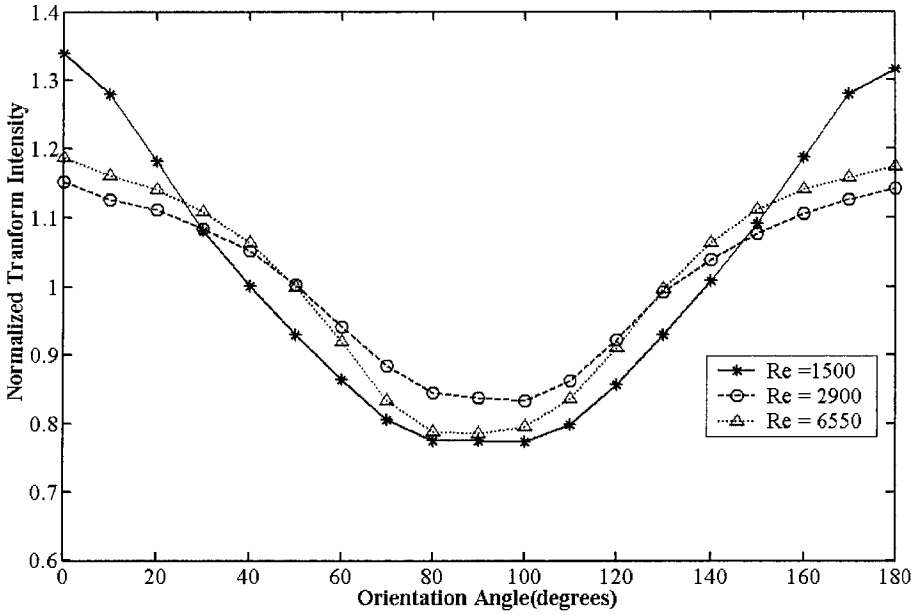

Figure 4-23. Fibre orientation distribution of 10 mm cut hemp fibres

Figure 4-24 shows the standard deviation corresponding to each point in Figure 4-23. The standard deviation for all the points in Figure 4-23 is higher than corresponding points in Figure 4-18. This could be due to the increase in hydroentanglement of hemp fibres with increase in fibre length.

In both Figures 4-18 and 4-23, the standard deviation decreases with increase in Reynolds number because of decrease in instances of fibre hydroentanglement with increase in flow rate.

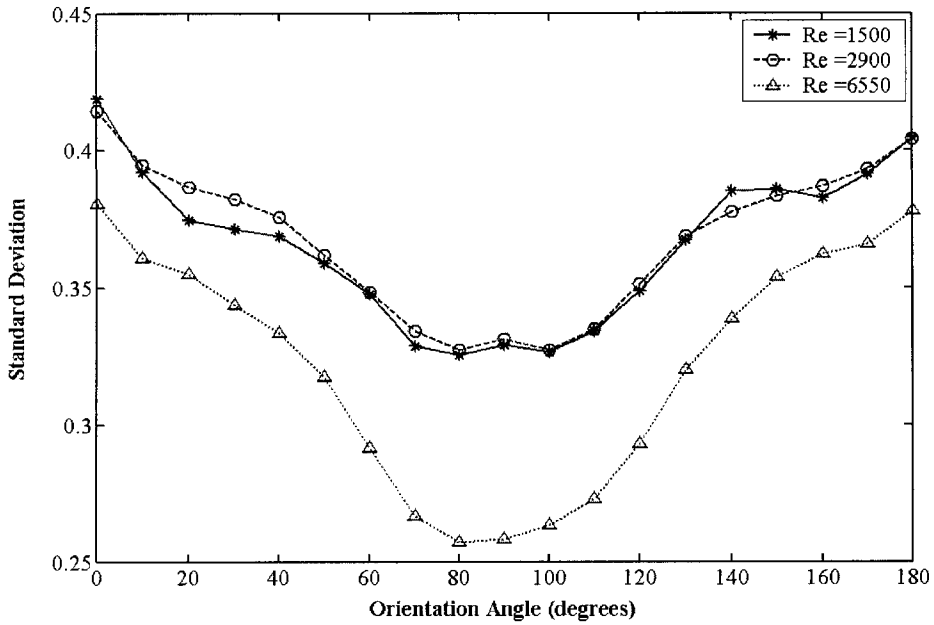

Figure 4-24. Standard deviation for various points in Figure 4-23.

Fibre orientation distribution was not calculated for hemp fibre suspensions containing hemp fibres longer than 10 mm because of the tendency of longer fibres to form loops, which give erroneous orientation value.

Chapter 5. Conclusions

The friction factor curves derived from pressure drop and flowrate reading can be used to detect the hydroentanglement of hemp fibres. High fluctuation in pressure drop was detected for high consistency and long fibre lengths. Fluctuation in pressure drop tends to subside with increase in flow rate for all consistencies and fibre lengths.

The intensity method can be used to detect as well as measure the severity of hydroentanglment of hemp fibres at low consistencies. Moreover, the intensity method make it possible to differentiate between fibre flocs which were caused due to the entanglement of thin fibres with coarse fibres from the one caused by hydroentanglement of thin fibres with each other. Hydroentanglement instances for hemp fibres increased with fibre cutting until the fibre length was reduced to 5mm. Hydroentanglement instances per unit mass decreased with increase in flow rate for all fibre lengths. Size of fibre flocs in fibre suspension decreased with shortening of long fibres and lowering of consistency. Higher flow rate results in smaller size of fibre flocs.

Fourier transform method was successfully used to find the mean angle of orientation for natural fibres. For both softwood and hemp fibres it was found that most of the fibres were aligned in the flow direction for laminar flow and more randomly aligned for turbulent flow regime. Hydroentanglment of hemp fibres increased the standard deviation of the distribution.

Chapter 6. Future Work

In this study the temperature of the slurry was kept close to the room temperature. Thus, the effect of temperature on the hydroentanglement of fibres should be studied in future work.

Bubble mixing system used in this study is not usually used for pulp mixing in paper industry. Thus, some other method of mixing, which doesn't assist in fibre hydro entanglement, needed to be found.

In a headbox, fibres are spread over the paper machine using nozzles. The effect of geometry of nozzles on hydroentanglement and fibre orientation should be studied in the future.

References

[1] Jeyasingam, J.T., "Industrial experience in the Manufacture of cigarette tissue using hemp pulp", Proceedings TAPPI Pulping Conference, 485-497(1993).

[2] Balde, S., "Fibre production in Alberta-new ideas", Field of Fibre Symposium, PAPTAC Nonwood Fibre Committee (2003)

[3] Lokken, J., "Developing Representative Composite Samples of Fields and Bales of Flax Straw", Field of Fibre Symposium, PAPTAC Nonwood Fibre Committee (2003).

[4] Hurter, R.W., "Agricultural Residues", TAPPI Nonwood Fibers Short Course (1997).

[5] Smook, G.A., "Handbook for Pulp and Paper Technologists", Angus Wilde Publications Inc, 2002.

[6] Mason, S.G., "The Motion of Fibers in Flowing Liquids", Pulp & Paper Mag.Can., 51(5): 93-100(1950).

[7] Mason, S.G., "Fibre Motions and Flocculation", Pulp & Paper Mag.Can. 55 (12): 96-102(1954).

[8] Forgacs, O.L., Robertson, A.A. and Mason, S.G., "the Hydrodynamic Behavior of Paper making Fibres", Pulp & Paper Mag.Can., 59(2): 117-128(1958).

[9] Soszynski, R.M. and Kerekes, R.J., Nord.Pullp Paper Res.J, 4:172 (1988).

[10] Wollage, J.C., Technical Association Papers SeriesXXII, No.1 (1939).

[11] Kerekes, R.J., "Pulp Flocculation in Decaying Turbulence: A Literature Review", J. Pulp & Paper Science, 9(3): TR86 (1983).

[12] Chang, M.Y., and Robertson, A.A., "Flocculation Studies of Fibre Suspensions: Influence of Zeta Potential", Pulp & Paper Mag.Can. , 68(9): T438 (1967).

[13] Robertson, A.A. and Mason, S.G., "The Flow Characteristics of Dilute Fiber Suspension", TAPPI J., 40(5): 326-334 (1957).

[14] Kerekes, R.J., Soszynski, R.M. and Tam Doo, "The Flocculation of Pulp Fibres", 8th Fundamental Research Symposium, Oxford, 1:265 (1985).

[15] Kerekes, R.J. and Schell, C.J., "Characterization of fibre Flocculation Regimes by a Crowding factor", J.Pulp & Paper science, 18(1): J32-J38 (1992).

[16] Dodson, C.T.J., "Fiber crowding, fiber contacts, and fiber flocculation", TAPPI J., 79(9): 211-215 (1996).

[17] Ullmar, M. and Norman, B., "Observation of Fiber Orientation in a Headbox Nozzle at low Consistency", Proceeding TAPPI Engineering & Papermakers Conference, 865-874 (1997).

[18] Ghassemieh, E., Versteeg, H.K. and Acar, M.., "Microstructural Analysis of Fiber Segments in Nonwoven Fabrics using SEM and Image processing", INJ, 26-31 (2001).

[19] Russ, J.C., "The Image Processing Handbook", CRC Press, 1999.

[20] Jain, A.K., "Fundamentals of digital Image Processing", Prentice–Hall Inc.,1989.

[21] Pourdeyhimi, B., Dent, R. and Davis, H., "Measuring Fiber Orientation in Nonwovens PartIII: Fourier Transform", Textile Res. J., 67(2):143-151(1997).

[22] Pourdeyhimi, B., Dent, R., Jerbi, A., Tanaka, S. and Deshpande, A., "Measuring Fiber Orientation in Nonwovens Part V: Real Webs", Textile Res. J., 69(3):185-192 (1999).

Appendix [A]

A.1. Flow equipment

A.1.1. DPCell (Differential Pressure Cell)

Manufacturer:	Rosemount
Model:	3051CD, Differential pressure transmitter
Total Performance:	± 0.15% of span
Reference Accuracy:	± 0.1% of span
Output:	4-20mA dc with Hart Protocol

A.1.2. Magnetic Flowmeter

Manufacturer:	Foxboro Canada Inc
Model:	M/2800 Series Magnetic Flowtube
Nominal Line Size:	6mm
Flow measurement range:	0 to19 L/min

Normal operating temperature: -10 to +50 ^{o}C

A.1.3.Progressive cavity pump

Manufacturer:	Cole-Parmer Instrument Company
Model:	Masterflex Quick Load Pump
Flow capacity:	0.06 to 2300 ml/min
Max rpm:	600

Normal operating temperature: -20 to 40 ^{o}C

A.2. Imaging equipment

A.2.1.Computer

P4 2.4GHz, 15" monitor

A.2.2.Camera

Manufacturer:	Sentech
Model:	STC-1100B, monochrome CCD
Picture element:	1/3"
Image size:	649(H)×494(V) pixels
Setting:	
Scanning mode:	Double speed progressive scan
Gamma:	0.45/1.0
S/N Ratio:	>56 dB (Gain off)
Shutter speed:	1/8000 sec

A.2.3. Lens

25 mm 1:1.4 Cosmicar Pentex TV lens

A.2.4. Light

Schott –Fostec 2"×2" back light

A.2.5. Image Acquisition Software

IO Industries Video Savant Basic 4.0

A.2.6. Image Processing Software

MATLAB 6.5 Image Processing Toolbox

Appendix [B]

B.1. MATLAB Program for implementing Intensity method

```
% Intensity method - By Sandeep Randhawa
 clear all;
% INPUT DATA
% " ----------------------------------------------------------------
S = 0; % OR use: input (' Enter START image number: ');
E = 5000; % OR use: input (' Enter END image number: ');
path='C:\Documents and Settings\Sandeep\My Documents\My Pictures\New
Folder\test\test_';
pathsave='C:\Documents and Settings\Sandeep\My Documents\My Pictures\New
Folder\Saved_';
step = 1; % If you want to see images at a certain interval
% ---------------------------------------------------------------- "
disp ('Program running, please wait ....');
% Opening file for storing Data
fid = fopen ([pathsave, 'Data.dat'], 'w');
Nf = 0;
for fn = S: step : E,
   Nf = Nf + 1;
   disp(['Image # ' int2str(fn)]);
   fns = int2str(fn);
```

```
% Individual File Name for Images
% " ------------------------------------------------------------------
switch length(fns)
case 1
    fn_prf = [path '000' fns '.jpg'];
  case 2
    fn_prf = [path '00' fns '.jpg'];
  case 3
    fn_prf = [path '0' fns '.jpg'];
otherwise
    fn_prf = [path  fns '.jpg'];
  end
  % ------------------------------------------------------------------ "
  % Reading Current Image
  im = imread (fn_prf);
  %Cropping image to desired size
  ic=imcrop (im,[0 40 659 230]);
  id=im2double(ic);
 %-------------------------------------------------------------------
  %Reading Background image and cropping to desired size
   b = imread ('B.jpg');
    bc = imcrop (b,[0 40 659 230]);
    bd = im2double (bc);
```

```
%-----------------------------------------------------------------------
%Dividing image with background
 D=imdivide(id,bd);
 %-----------------------------------------------------------------------
% Plotting current image
figure (1);
imshow (D,[]); title(['Image # ', fns]);
pause (1);
im_mean(Nf) = mean2(D);
 im_std(Nf) = std2(D);
 end
[x,y]=size(im_mean);
im_meannew=ones(x,y)-im_mean;
%Difference of mean intensity and standard deviation for each image frame
% with mean differnce for whole file removed
diff=(im_meannew-mean(im_meannew))-(im_std-mean(im_std));
fprintf(fid, '%7.3f  %7.3f %7.3f \n',[ im_meannew; im_std;diff] );
fclose(fid);
```

Appendix[C]

C.1. MATLAB Program for implementing Fourier transform method

```
% Fourier transform method- By Sandeep Randhawa
 clear all;
% INPUT DATA
% " ----------------------------------------------------------------
S = 0; % OR use: input(' Enter START image number : ');
E = 5000; % OR use: input(' Enter END image number : ');
path = 'C:\Documents and Settings\Sandeep\My Documents\My Pictures\New
Folder\test\test_';
pathsave='C:\Documents and Settings\Sandeep\My Documents\My Pictures\New
Folder\SavedF_';
step = 1; % If you want to see images at a certain interval
% ---------------------------------------------------------------- "
disp ('Program running, please wait ....');
% Opening file for storing Data
fid = fopen ([pathsave, 'Data.dat'], 'w');
Nf = 0;
for fn = S: step : E,
   Nf = Nf + 1;
   disp(['Image # ' int2str(fn)]);
    fns = int2str(fn);
```

```
    % Individual File Name for Images
   % " ------------------------------------------------------------------
switch length(fns)
case 1
       fn_prf = [path '000' fns '.jpg'];
case 2
      fn_prf = [path '00' fns '.jpg'];
 case 3
      fn_prf = [path '0' fns '.jpg'];
otherwise
      fn_prf = [path fns '.jpg'];
   end
   % ------------------------------------------------------------------ "
%  fn_prf = [path '0' fns '.jpg'];
   % Reading Current Image
   im =  imread (fn_prf);
   %Cropping image to desired size
   ic= imcrop (im,[50 80 500 220]);
   id=im2double(ic);
%-------------------------------------------------------------------------
   %Reading Background image and cropping to desired size
    b= imread('B.jpg');
     bc= imcrop (b,[50 80 500 220]);
```

```
    bd= im2double(bc);
    sbc=size(bc)
%-----------------------------------------------------------------
 % Dividing image with background
  D= imdivide (id,bd);
  Sd =size(D)
%-----------------------------------------------------------------
 %Edge detection with manually selected threshold values
[BW]=edge (D, 'canny', [0.17 0.1719] );
% Plotting current image
 figure (1);
 imshow (BW); title(['Image # ', fns]);
 pause (1);
%-----------------------------------------------------------
 %Calculating Fourier transform
  F= fft2 (BW);
 %-------------------------------------------------------------------------
 % Quadrant swapping to bring centre to zero
 Fs= fftshift (F);
 Fs2= (abs(Fs));
 sz=size(Fs2)
%   figure,imagesc(Fs2),colorbar
%-----------------------------------------------------------------
```

```
% Changing cartissen coordinates to polar coordinates for slicing
   pim =  polartrans (Fs2,200,360);
   size (pim);
    figure,imagesc(pim),colorbar
% ------------------------------------------------------------------------------
for i = 0:1:18
  if i= = 0
  pimne( i+1)= (mean(mean(pim(50:150,90:95)))+mean(mean(pim(50:150,270:275))))/2;
  elseif i <9
   pimne( i+1)= (mean(mean(pim(50:150,(95+(i-2)*10):(95+(i-2)*10+10))))
                  +mean(mean(pim(50:150,(275+(i-2)*10):(275+(i-2)*10+10)))))/2;
  elseif i = =9
  pimne(i+1) = (mean(mean(pim(50:150,[355:360,1:5])))
                   + mean(mean(pim(50:150,175:185)) ))/2 ;
  elseif I <18 & I >9
  pimne(i+1) =(mean(mean(pim(50:150,5+(i-2)*10:5+(i-2)*10+10)))
                 +mean(mean(pim(50:150,185+(i-2)*10:185+(i-2)*10+10))))/2;
  elseif  i  = =18
 bpim(i+1) = (mean(mean(pim(50:150,85:90)))+mean(mean(pim(50:150,265:270))))/2;
  end
 end
  pimnew(Nf:Nf+18)=pimne;
  Nf=Nf+18;
```

```
end
%-------------------------------------------------------------------------
fprintf(fid, '%7.3f \n', pimnew );
fclose(fid);
```

C.2. MATLAB Program for transforming image to polar coordinates

```
% POLARTRANS - Transforming image to polar coordinates
%       im    - image to be transformed.
%       nrad  - number of radius values.
%       ntheta - number of theta values.
%       cx, cy - optional specification of origin.  If this is not
%             specified it defaults to the centre of the image.

%       shape  - optional string 'full' or 'valid'
%             'full' results in the full polar transform being
%             returned (the circle that fully encloses the original
%             image). This is the default.
%             'valid' returns the polar transform of the largest
%             circle that can fit within the image.
%  pim    - image in polar coordinates with radius increasing
%             down the rows and theta along the columns. The size
%             of the image is nrad x ntheta.  Note that theta is
%             +ve clockwise as x is considered +ve along the
%             columns and y +ve down the rows.

% When specifying the origin it is assumed that the top left pixel has
% coordinates (1,1).
```

```
function pim = polartrans(im, nrad, ntheta, cx, cy,shape)
[rows, cols] = size(im);
if nargin==3        % Set origin to centre.
   cx = cols/2+.5;  % Add 0.5 because indexing starts at 1
   cy = rows/2+.5;
end

if nargin < 6, shape = 'full'; end
if strcmp(shape,'full')        % Find maximum radius value
   dx = max([cx-1, cols-cx]);
   dy = max([cy-1, rows-cy]);
   rmax = sqrt(dx^2+dy^2);
elseif strcmp(shape,'valid')   % Find minimum radius value
   rmax = min([cx-1, cols-cx, cy-1, rows-cy]);
else
   error('Invalid shape specification');
end

% Increments in radius and theta
deltatheta = 2*pi/ntheta;
deltarad = rmax/(nrad-1);
   [theta, radius] = meshgrid([0:ntheta-1]*deltatheta, [0:nrad-1]*deltarad);
xi = radius.*cos(theta) + cx;  % Locations in image to interpolate data
```

```
yi = radius.*sin(theta) + cy;  % from.

[x,y] = meshgrid([1:cols],[1:rows]);

pim = interp2(x, y, double(im), xi, yi);
```